ERDC TR-17-6

US Army Corps
of Engineers®
Engineer Research and
Development Center

ERDC
INNOVATIVE SOLUTIONS
for a safer, better world

Army Environmental Quality Technology

Validation of Short-Term Noise Assessment Procedures

FY16 Summary of Procedures, Progress, and Preliminary Results

Michelle E. Swearingen, Gregory W. Lyons, Kate A. Morozova,
Andrew R. Lammers, Brian R. Greene, Michael J. White,
Lacey S. Duckworth, and Jesse M. Barr

June 2017

Construction Engineering
Research Laboratory

The U.S. Army Engineer Research and Development Center (ERDC) solves the nation's toughest engineering and environmental challenges. ERDC develops innovative solutions in civil and military engineering, geospatial sciences, water resources, and environmental sciences for the Army, the Department of Defense, civilian agencies, and our nation's public good. Find out more at www.erdc.usace.army.mil.

To search for other technical reports published by ERDC, visit the ERDC online library at http://acwc.sdp.sirsi.net/client/default.

Validation of Short-Term Noise Assessment Procedures

FY16 Summary of Procedures, Progress, and Preliminary Results

Michelle E. Swearingen, Gregory W. Lyons, Kate A. Morozova, Andrew R. Lammers, Brian R. Greene, Michael J. White, and Jesse M. Barr

Construction Engineering Research Laboratory
U.S. Army Engineer Research and Development Center
2902 Newmark Drive
PO Box 9005
Champaign, IL 61826-9005

Lacey S. Duckworth

Information Technology Laboratory
U.S. Army Engineer Research and Development Center
3909 Halls Ferry Road
Vicksburg, MS 39180-6199

Final report

Prepared for Assistant Secretary of the Army for Installations, Energy and Environment (ASA(IE&E))
110 Army Pentagon, Room 3E464
Washington, DC 20310-0110

Under Work Unit 2JF1C8, “Short-Term Noise Assessment Procedures.”

Abstract

Army regulations require that installations assess the impacts of training range noise on wildlife and the human community. This work provides a summary of the work performed in fiscal year (FY) 2016 for the Environment, Safety and Occupational Health Short-Term Noise Assessment Procedure Demonstration/Validation project. This report describes the procedure used to generate the noise models' output dataset, and then it compares that dataset to the benchmark, the Engineer Research and Development Center's Long-Range Sound Propagation dataset. It was found that the models consistently underpredict the measured values. Multiple topics were explored towards identifying possible sources of error. The peak-level calculation algorithm is found to perform adequately, but an alternative method is recommended for future use. Significant meteorological variability is found across the landscape, leading to challenges in estimating the correct propagation class for a particular scenario. A deeper investigation of the propagation class selection algorithm is continuing in FY17. Updates to the noise assessment tools are identified. Throughout this document, procedures used for calculations and analysis are included.

Contents

Figures and Tables

Figures

Tables

Preface

This study was conducted for Office of the Assistant Secretary of the Army for Installations, Energy and Environment (ASA(IEE)) under program element E21, "Army Environmental Quality Technology," Work Unit 2JF1C8, "Short-Term Noise Assessment Procedures." The sponsor's technical monitor was Ms. Amy Borman.

This work was conducted by the Ecological Processes Branch of the Installations Division (CEERD-CNN), U.S. Army Engineer Research and Development Center, Construction Engineering Research Laboratory (ERDC-CERL). Dr. Chris Rewerts was Chief, CEERD-CNN; Ms. Michelle J. Hanson was Chief, CEERD-CN; and Mr. Alan Anderson was the Technical Director for Sustainable Ranges and Lands, CEERD-CZT. The Deputy Director of ERDC-CERL was Dr. Kirankumar V. Topudurti, and the Director was Dr. Ilker R. Adiguzel.

Work was also conducted by the CAD/BIM Technology Center (CEERD-ISC) of the Software Engineering and Informatics Division (CEERD-IS) of the ERDC Information Technology Laboratory (ERDC-ITL). Mr. Edward L. Huell Jr. was Chief, CEERD-ISC; Mr. C.K. (Ken) Pathak was Chief, CEERD-IS. The Deputy Director of ERDC-ITL was Ms. Patti S. Duett, and the Director was Dr. Reed L. Mosher.

The Commander of ERDC was COL Bryan S. Green, and the Director was Dr. David W. Pittman.

Unit Conversion Factors

Multiply	By	To Obtain
degrees (angle)	0.01745329	radians
miles (U.S. statute)	1,609.347	meters
pounds (mass)	0.45359237	kilograms

1 Introduction

1.1 Background

The U.S. Army is required to assess the impacts of training range noise on wildlife and the human community (AR 200-1, Chapter 14). The ESOH (Environment, Safety and Occupational Health) Impacts of Short-Term Noise Assessment Procedures project was initiated by the Environmental Technology Office, Office of the Assistant Secretary of the Army for Installations, Energy and Environment (ASA(IE&E)) to validate the short-term noise assessment procedures that are currently used by the U.S. Army. The Army currently uses an annual average noise-level metric to assess the impact of military training and testing activities on surrounding communities (AR 200-1, Chapter 14). This approach was derived from approaches commonly used in nonmilitary applications such as the transportation sector and represents methods approved by the National Research Council Committee of Hearing, Bioacoustics, and Biomechanics. However, due to the unique characteristics of weapons-system blast noise, average noise assessment criteria can significantly under- or over-estimate the impact of military activities on surrounding communities and those estimation errors can impact siting and operation of ranges. This estimation problem arises because weapons noise is very short in duration (impulsive), somewhat infrequent, and very loud. For unusual events or increased training tempo, improved short-term noise assessments will provide Army installations with a means to better communicate the impact of the temporary noise environment to the community. Additionally, normal operations will also benefit from more robust short-term noise assessments, as these values are commonly used as a supplemental metric. Accurate noise assessments that take expected meteorological conditions into consideration are valuable for protecting the training mission.

1.2 Objective

The purpose of this work is to demonstrate and validate technologies for making improved short-term noise assessments of Army blast noise. This work includes validating the underlying computational algorithms, databases, and procedures of existing noise software, as well as providing required training materials to support technology transition.

1.3 Approach

This project will test and validate the software and underlying algorithms that the Army uses to predict short-term noise levels due to training and testing activities. The outputs of currently used software tools—BNoise2™ (Blast Noise Version 2; Swearingen 2017), SARNAM™ (Small Arms Range Noise Assessment Model; Pater 2007), and RMTK (Range Managers Toolkit) Noise Tool (Swearingen 2006)—will be compared to multiple operational datasets, to include a highly controlled benchmark dataset and noise measurements collected during normal training operations at several Army installations. Any deficiencies will be corrected. Upon completion of the validation, a set of online, self-guided training materials will be developed to educate the Army's training community about the appropriate use and interpretation of noise models and their outputs.

1.4 Scope

This technical report provides a summary of the work performed in fiscal year (FY)16 for this project. This report covers the following tasks from the scope of work:

1. Description of the procedure used to generate the model output dataset (Chapter 2).
2. Statistical analysis of a comparison between the benchmark dataset (ERDC [Engineer Research and Development Center] Long-Range Sound Propagation Dataset, described in Pater et al. 2017) and the model outputs for corresponding meteorological conditions (Chapter 3).
3. Discussion of the peak-level calculation algorithm and comparison of its results to other methodologies (Chapter 4).
4. Analysis of the meteorological conditions and mapping those conditions to selected propagation conditions within the noise models (Chapter 5).
5. Overview of the progress toward updating the noise assessment models (Chapter 6).
6. Overview of Army participation in Navy webinar training (Chapter 7), used to partially fulfill training aspect of project.

2 Model Data Generation Procedure

The primary goal of the Short-Term Noise Assessment Procedures Demonstration/Validation project is to validate that the suite of noise assessment models for military range noise (BNoise2, SARNAM, and RMTK Noise Tool) provide output that matches measurements to within acceptable error limitations. Due to the inherent variability in sound propagation through the atmosphere, resulting from atmospheric turbulence and the uncertainty of conditions along the sound path (Valente 2012), the measured values at noise monitors are not expected to exactly match the model outputs.

In FY16, the model output was compared to the benchmark—the ERDC Long-Range Sound Propagation dataset. This curated dataset includes acoustic signals (waveforms, 1/3-octave band spectra, peak levels, and unweighted and C-weighted sound exposure levels) collected at distances of up to 16 km and in three different directions from a central, controlled source (1.25 lb Composition C-4 explosive). Time-synchronized meteorological data from a 15-meter high instrumented tower is processed into propagation conditions that correspond to the noise assessment tool single-event propagation classes for each acoustic measurement. Every acoustic signal in the dataset has been verified as being a blast signature. Some recordings that could not be identified as blast were not included in these analyses (Valente et al. 2012b).

Noise assessment model output was produced that corresponds to the propagation conditions and distances in the controlled experimental dataset (Pater 2017). For each of the propagation tables, a BNoise2 case file was generated using an explosion of 1.25 lb Composition C-4 as the sound source. The receiver grid was defined as 125 m wide and 16,000 m long, with a grid cell spacing of 125 m. This grid configuration allowed easy extraction of the levels generated at horizontal ranges corresponding to the measurements (125 m, 1 km, 2 km, 4 km, 8 km, 12 km, and 16 km). A set of case files was generated using these basic parameters and designating the use of each of the propagation tables at nine different directions (direction of propagation from source to receiver – direction of wind flow, 0 to 180 degrees) to capture the maximum number of conditions measured for comparisons; this allows examination of the effects of the vector component of wind flow in the direction of acoustic propagation. These sets of files were generated for the desert ground condition and the temperate

ground condition, which effectively are equivalent to packed sand and grass. A simple script was written that batch-runs BNoise2 by using the series of case files to automate the simulations and then placing the required information into a spreadsheet for later use. A sample of the generated spreadsheet information appears in Table 1.

Table 1. Example output from BNoise2 simulations. (Only one example ground type, stability class, wind speed, and azimuth combination is shown here.)

Ground Type	Stability Class	Wind Speed (m/s)	Azimuth (°)	Distance (m)	PK15 (dB)	PK50 (dB)	CSEL50 (dB)	ZSEL50 (dB)
Desert	B	0	0	125	148.5	145.5	118.4	120.4
Desert	B	0	0	500	128	123.5	102.9	105.7
Desert	B	0	0	1000	119.5	114	95.5	98.9
Desert	B	0	0	2000	111	104.5	87.7	91.8
Desert	B	0	0	4000	101	93	78.2	83.3
Desert	B	0	0	8000	90	80	68.5	75.1
Desert	B	0	0	12000	86	73.5	66.6	73.4
Desert	B	0	0	16000	83.5	70	66.3	73.2

The set of propagation tables for grass and desert surfaces include 15 different conditions, corresponding to the combinations of Pasquill stability class and wind speed. The six Pasquill stability classes, described in Table 2, categorize the buoyant stability of the atmosphere in terms of routine meteorological measurements (Pasquill 1974). For wind speeds greater than zero, there are separate propagation tables for upwind and downwind conditions.

Table 2. Relationship between Pasquill classes and atmospheric stability.

Atmospheric Stability	Pasquill Class
Highly Unstable or Convective	A
Moderately Unstable	B
Slightly Unstable	C
Neutral	D
Moderately Stable	E
Extremely Stable	F

Here, upwind is defined as propagation against the flow and in the wind direction, and downwind is defined as parallel to the flow and opposite to the wind direction. To model propagation for azimuths that are not exactly upwind or downwind and to take the inherent variability of wind directions into account, results are combined by using a weighted sum of conditions, as defined below:

$$w_D = 0.3 \cos \varphi + 0.5 \tag{1}$$

$$w_U = 1 - w_D \tag{2}$$

$$S(\varphi) = 10 \log_{10}\left(w_D 10^{D/10} + w_U 10^{U/10}\right) \tag{3}$$

where:

w_D and w_U are the weightings for downwind and upwind, respectively;
D and U are the CCSELs associated with the downwind and upwind directions, respectively; and
φ is the angle between the propagation direction and the downwind direction.

3 Statistical Analysis Comparing Model Output to Experimental Data

A detailed statistical analysis was performed to determine the goodness of fit of the model output to the experimental data. A complete description of this analysis follows.

3.1 Statistical tests for normality

Anderson-Darling and Shapiro-Wilk tests for normality (Razali and Wah 2011) were used to assess the normality of the population distributions. The following are the hypotheses for both tests:

- H_0: The population is normally distributed.
- H_1: The population is not normally distributed.

If the p-values are below a certain alpha (α) level (0.05 is the most commonly used α), the null hypothesis is rejected, indicating that the sample did not come from a normal distribution. Both tests have more power when the sample size is large (>100) and therefore are more likely to reject the null hypothesis. On the other hand, when the sample size is small (<12), there is too little power, and the results could be misleading. If the sample size is small, the test likely rejects the null hypothesis (that the distribution was normal) when in fact, the distribution was normal, but it was hard to determine from so few points. In our test set, ~85% of the groups had sample sizes larger than 12.

The data were grouped by combinations of ground type, Pasquill class, wind speed, distance, and azimuth. There was a total of 394 groups with n>3; the mean sample size was 41. Of the groups with n>3, 65.7% of those groups failed to reject the null hypothesis of Shapiro-Wilks test, and 67.8% of the groups failed to reject the null hypothesis of Anderson-Darling test. This means that ~66% of the data could be normally distributed. Figure 1 is the graphical representation of these results. The red line indicates that α = 0.05. All P-values that fall below the red line indicate a rejected null hypothesis.

Figure 1. Results of normality tests, with Shapiro-Wilks test results on the left and Anderson-Darling test results on the right.

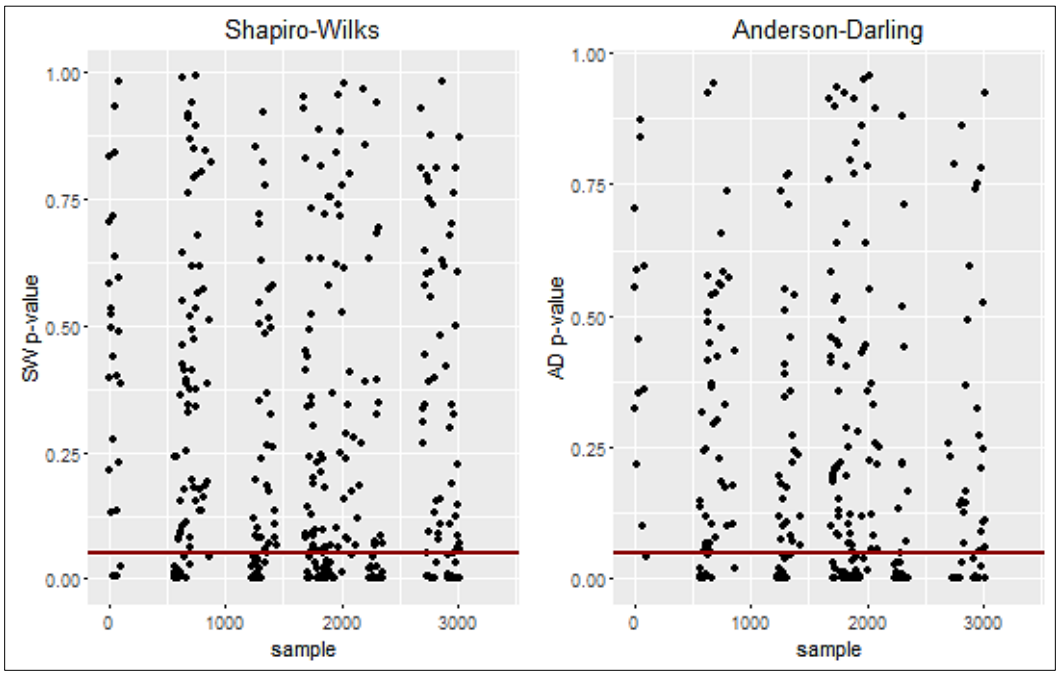

The three plots shown in Figure 2 are examples of the distribution commonly seen in the groups. It is obvious that these three examples are not from a normal distribution; most of the total of 394 groups are skewed.

Figure 2. Distributions of peak level in decibel (Lpk) from three sample groups.

Sample A: Pasquill Class D, Wind Speed = 2 m/s, Distance = 2 km, Azimuth = 112.5°, Desert condition. Sample B: Pasquill Class F, Wind Speed = 0 m/s, Distance = 2 km, Azimuth = 135°, Grass condition. Sample C: Pasquill Class F, Wind Speed = 0 m/s, Distance = 16 km, Azimuth = 157.5°, Grass condition.

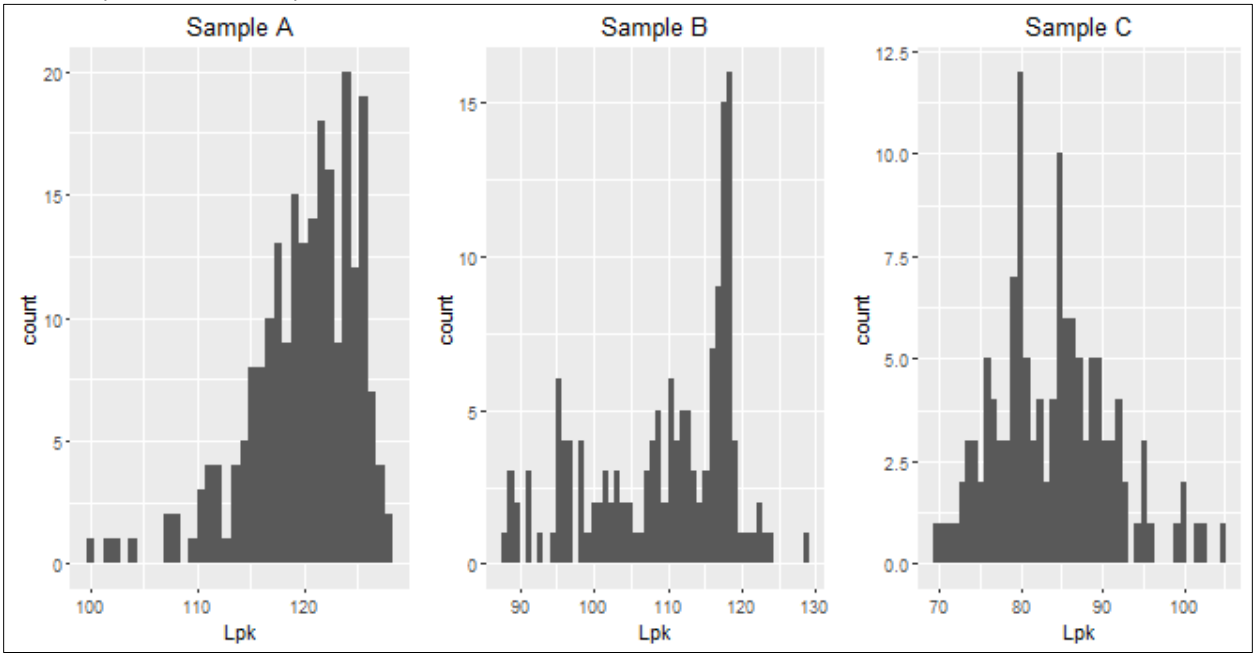

3.2 Model results

Several data preparation steps were necessary before the experiment data could be compared to the model data. Observations that did not have a meteorological measurement near to the propagation path were omitted. Measured conditions that did not match the model data (e.g., Stability Class A) were omitted as well. Wind speed values were converted to categories (0, 2, 4, 6, and 8 m/s) and azimuth values were converted to be on a scale from 0 to 180 degrees in increments of 22.5 degrees. Then, for each observation, *delta* (Δ) values were calculated using the following formula:

$$\Delta = O_i - E_i, \tag{4}$$

where:

O_i is the observed value
E_i is the expected value

The three histograms in Figure 3 show the overall distributions of the delta values for the three target variables: Lpk (peak level in dB), CSEL (C-weighted sound exposure level in decibels [dB]), and SEL (sound exposure level in dB). The shapes of the distributions are roughly symmetrical; however, they are not centered on zero. Table 3 shows the distribution characteristics, which confirms that the L_{pk}, CSEL, and SEL values are being underestimated by the model the majority of the time. At 11.88 decibels (dB), the mean of L_{pk} deviations is almost twice the mean of CSEL and SEL deviations.

Figure 3. Overall distributions of delta values for the three target variables.

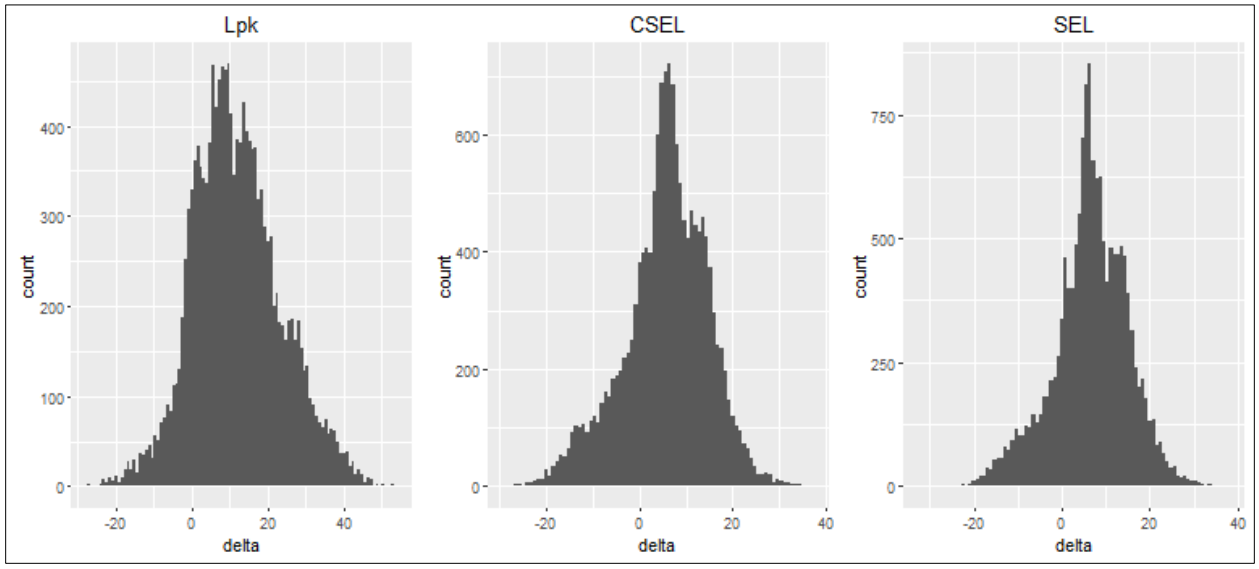

Table 3. Numerical representation of the distributions shown in Figure 3.

	Min	1st Q	Median	Mean	3rd Q	Max	SD
Lpk (dB)	-27.51	3.88	10.84	11.88	19.03	53.81	11.57
CSEL (dB)	-28.60	0.73	6.25	5.71	11.88	37.10	9.03
SEL (dB)	-32.34	1.90	6.72	6.55	12.30	37.57	8.52

Chi-squared goodness of fit tests were performed on the observed and expected values with the following hypotheses:

- H_0: The model is a good fit for the data.
- H_1: The model is not a good fit for the data.

This chi-squared test is usually used to test how well a statistical model fits the data. The resulting p-value was very low, and the null hypothesis was rejected. To find the reason the model was not a good fit, the Delta values will be compared for all of the variables. The goal of this analysis is to see, for which variables, the Delta values have the largest mean or range (i.e., which variables are causing the largest deviation from the model data).

3.2.1 PK15

Only 15% of the experimental values should fall above the model PK15 (peak level that will only be exceeded 15% of the time, based on meteorological variability) value. From the above analysis, it is expected that this will not be true for the experiment data. In fact, 62.44% of the experiment data were above the PK15 values. This higher-than-expected percentage is explained by the fact that the model is an underestimate of the data and the distributions are skewed, as illustrated in the Figure 3.

3.2.2 Correlations

In order to quantify the relationship between the delta values and the variables, Pearson correlation coefficients (Rodgers and Nicewander 1988) were calculated for all of the variables. A negative value implies a negative correlation, whereas a positive value implies a positive correlation. Table 4 shows the correlation values for L_{pk} Δ, CSEL Δ, and SEL Δ, showing that most of the variables are not highly correlated. The highest correlation coefficient is for Distance and L_{pk} Δ. It indicates that at higher distances, there is a greater variation between the observed and expected values. It is also important to note that stability class is not significantly correlated to either variable of L_{pk}, CSEL, and SEL.

Table 4. Correlation values for Δ L_{pk}, Δ CSEL, and Δ SEL.

Variable	Δ L_{pk} Correlation	Δ CSEL Correlation	Δ SEL Correlation
Stability Class	0.070	0.064	0.048
Ground Type	-0.263	-0.261	-0.265
Wind Speed	0.121	0.034	0.079
Azimuth	0.281	0.228	0.226
Distance	0.403	-0.003	0.065

3.2.2.1 Ground type

The graphs in Figure 4 show the delta values grouped by ground type. The mean deviations from expected values are closer to zero for grass terrain than for desert.

Figure 4. Delta values grouped by ground type (grass: green, desert: red).

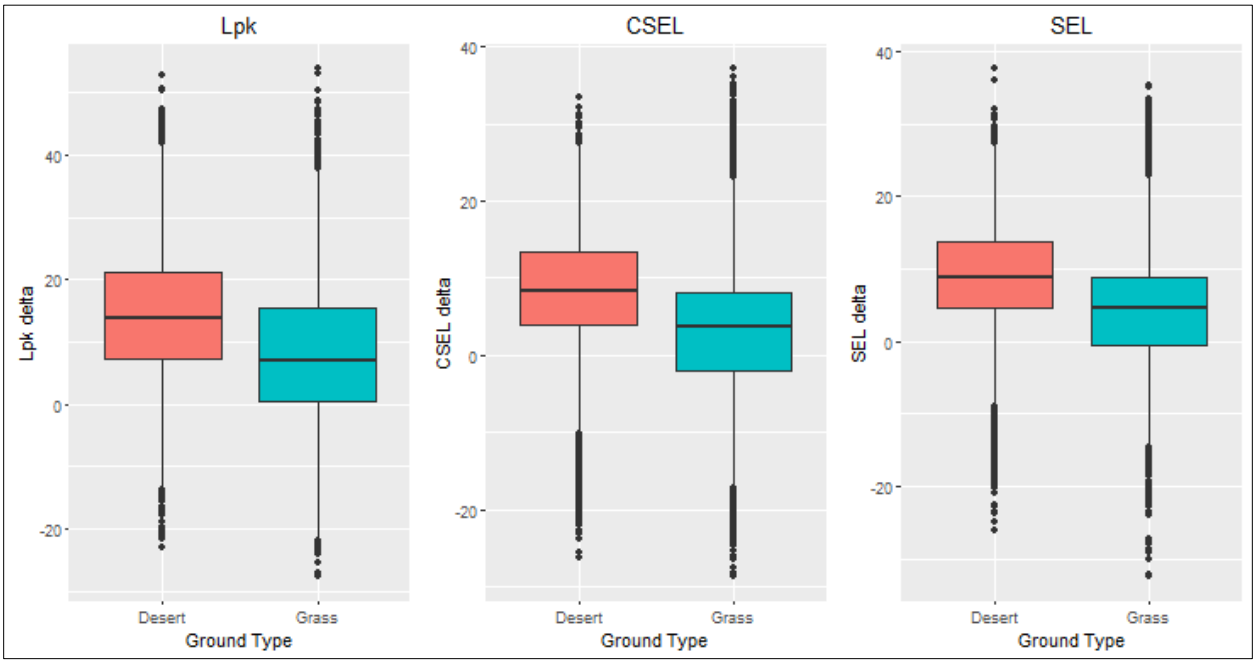

3.2.2.2 Stability class

The plots in Figure 5 show the distributions of delta values separated by ground type. Once again, grass terrain has smaller mean deviations than those for desert across all three variables. Stability Class E has a larger mean deviation and a larger range of deviations in L_{pk}. It is important to note that for grass terrain, there is significantly less variability across stability classes than for desert terrain.

3.2.2.3 Wind speed

As expected based on the previous examples shown, values for desert terrain are higher than those for grass terrain. The range of deviations shown in Figure 6 seems to decrease as wind speed increases, suggesting that the model is more accurate at higher wind speeds.

Figure 5. Delta distributions by stability class and ground type (grass: green, desert: red).

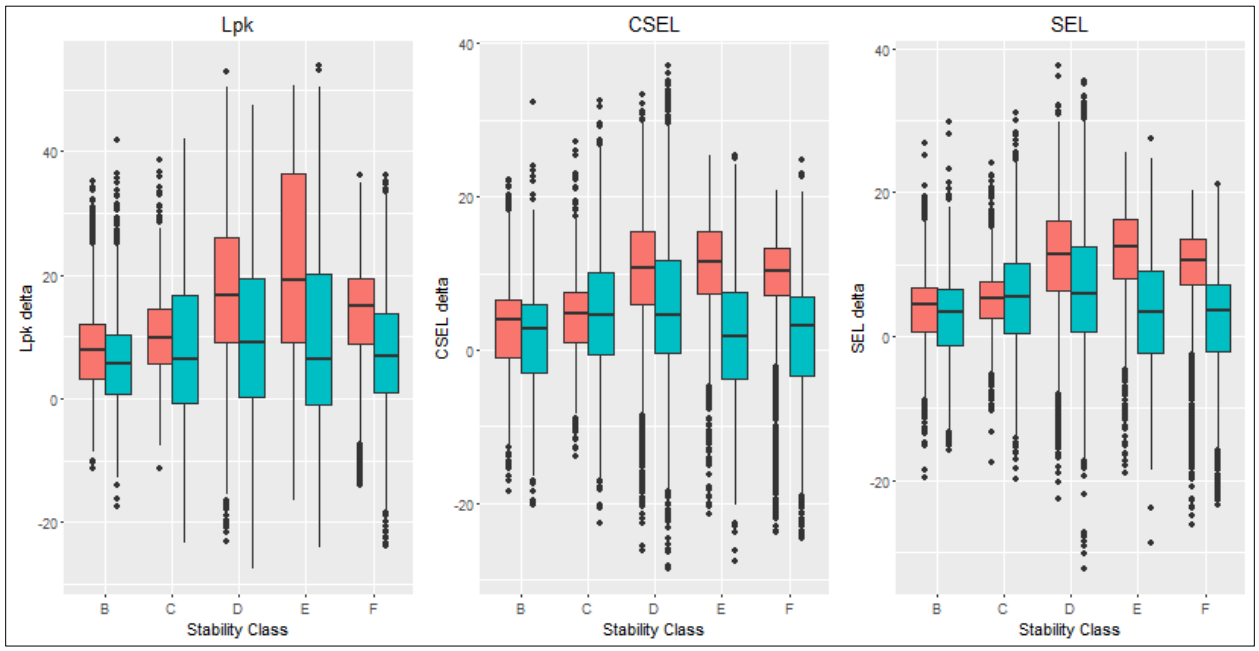

Figure 6. Delta distributions by wind speed.

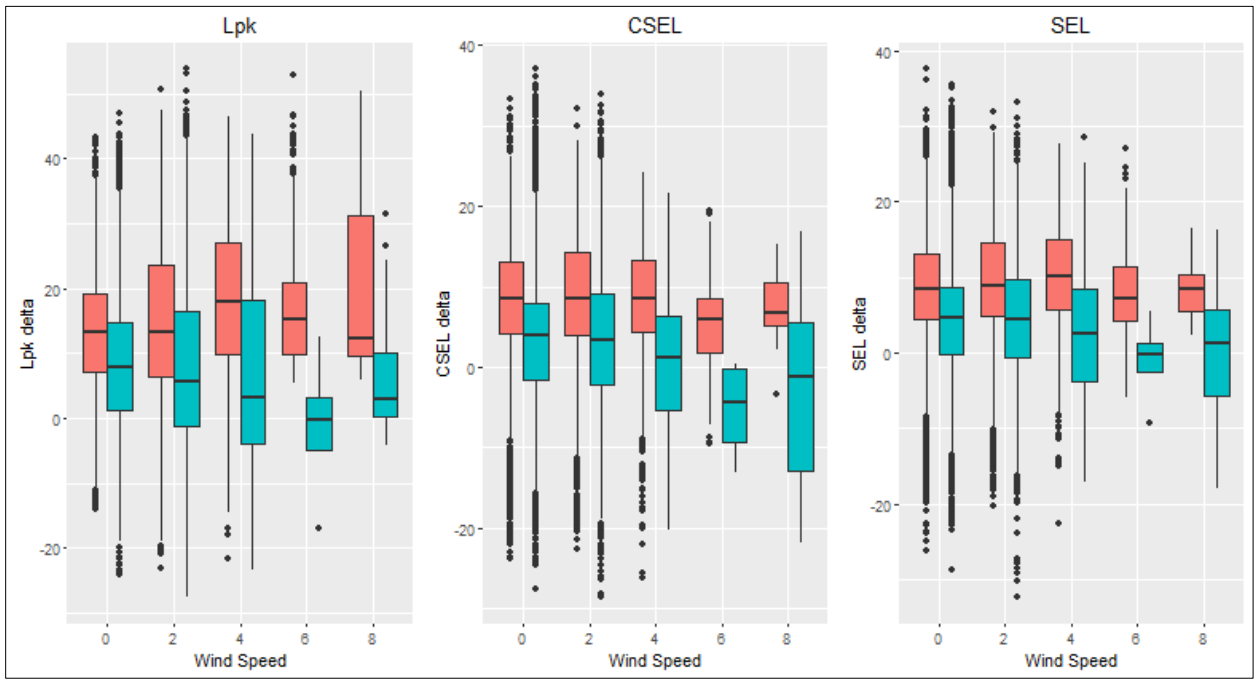

Azimuth

The only azimuth values associated with the desert terrain observations are 22.5° and 112.5°. Examining the raw data, it appears that there were prevailing winds from only two directions over the entire course of the study. Examining the results shown in Figure 7, there is a definite pattern to the delta values—ranges are smaller at Azimuth of 45°, 90°, and 135°. The means of the deltas increase to maximums of 112.5°. Considering that 180° is the upwind direction, this is not unaccountable, although the drop at 135° is unexplained.

Figure 7. Delta distributions by azimuth.

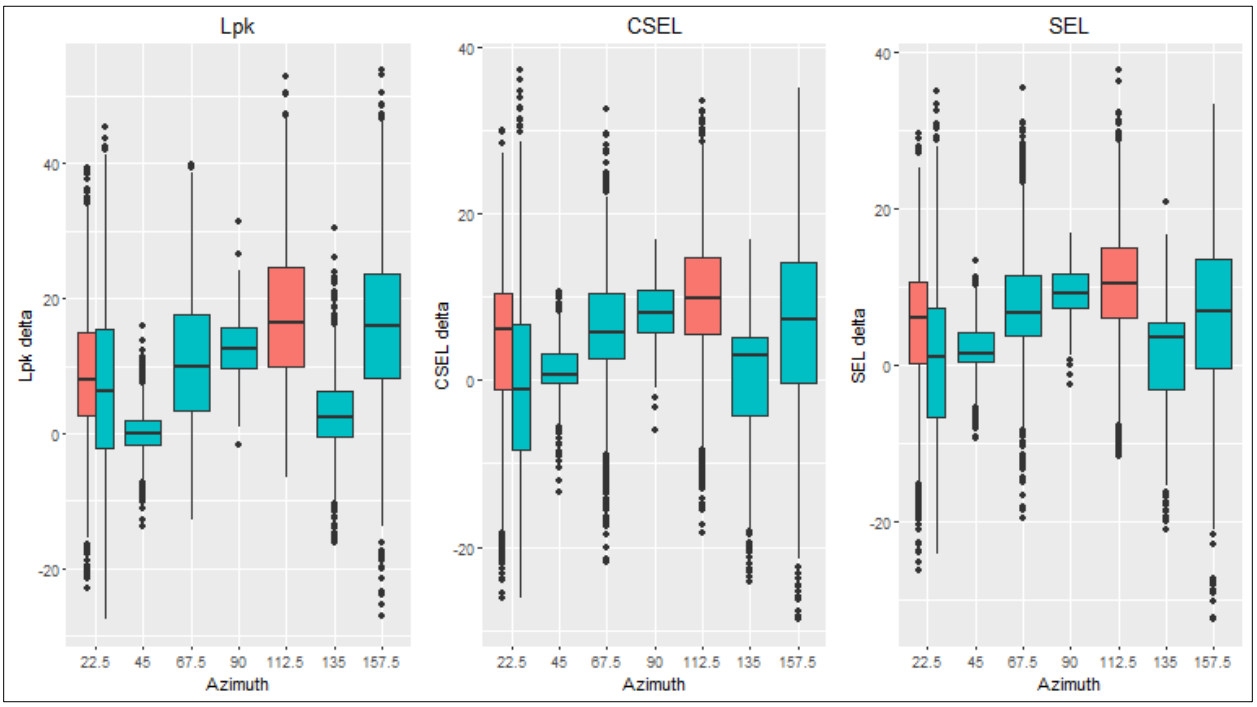

3.2.2.4 Distance

As shown in Figure 8, there is a definite pattern to the delta values separated by distance. There is less deviation from the model results at smaller distances. At 2 km and beyond, the range of the delta distributions also decreases as distance increases. It appears that the variability in the measured signals saturates around 4 km and does not increase substantially beyond this distance.

Figure 8. Delta distribution by distance.

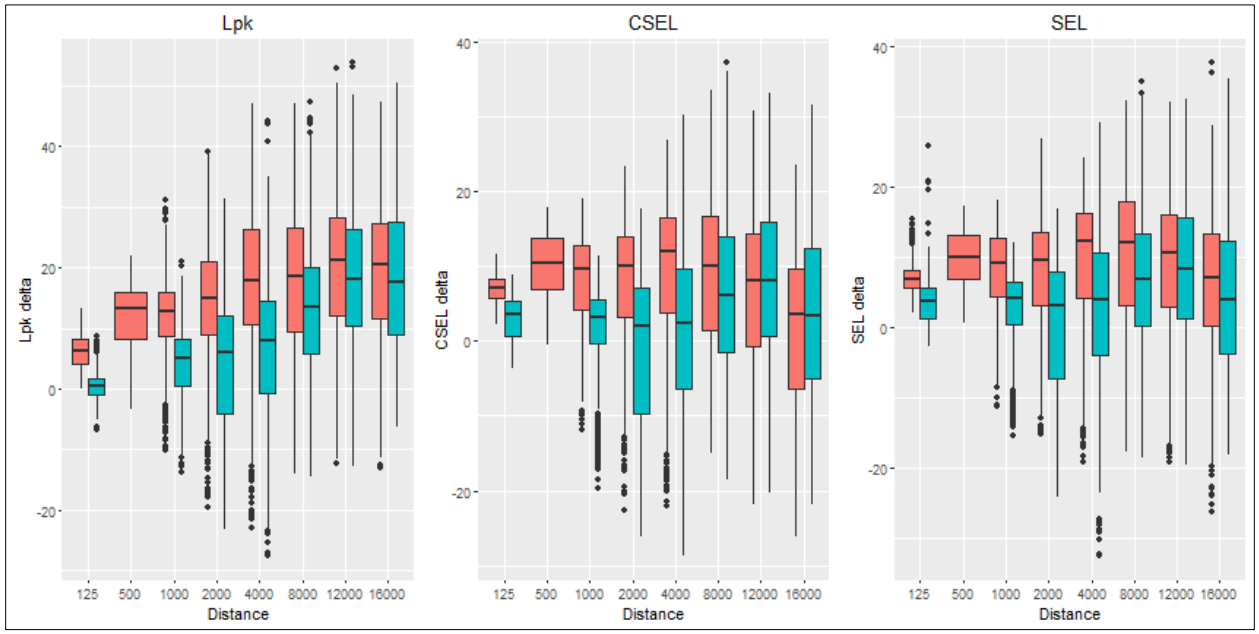

3.3 Further analysis

Since Lpk, CSEL, and SEL are highly correlated variables, only Lpk was chosen for further analysis. Figure 9 shows the distribution of deviations across the five stability classes, grouped by distance. At 125 m, the grass terrain has delta values with means close to zero, and little variation across stability classes. The desert terrain data is consistent with the observations made above—that the delta values are always larger than zero, suggesting that the model underestimates the observed data. Similar results are found at 1,000 m, 2,000 m, and 4,000 m. At higher distances (8,000 m, 12,000 m, and 16,000 m), neither of the terrains have means close to zero. While the delta values are almost always higher for desert terrain, both terrain types have a maximum delta in Stability Class E.

Figure 9. Delta distributions by Pasquill Stability Class and distance.

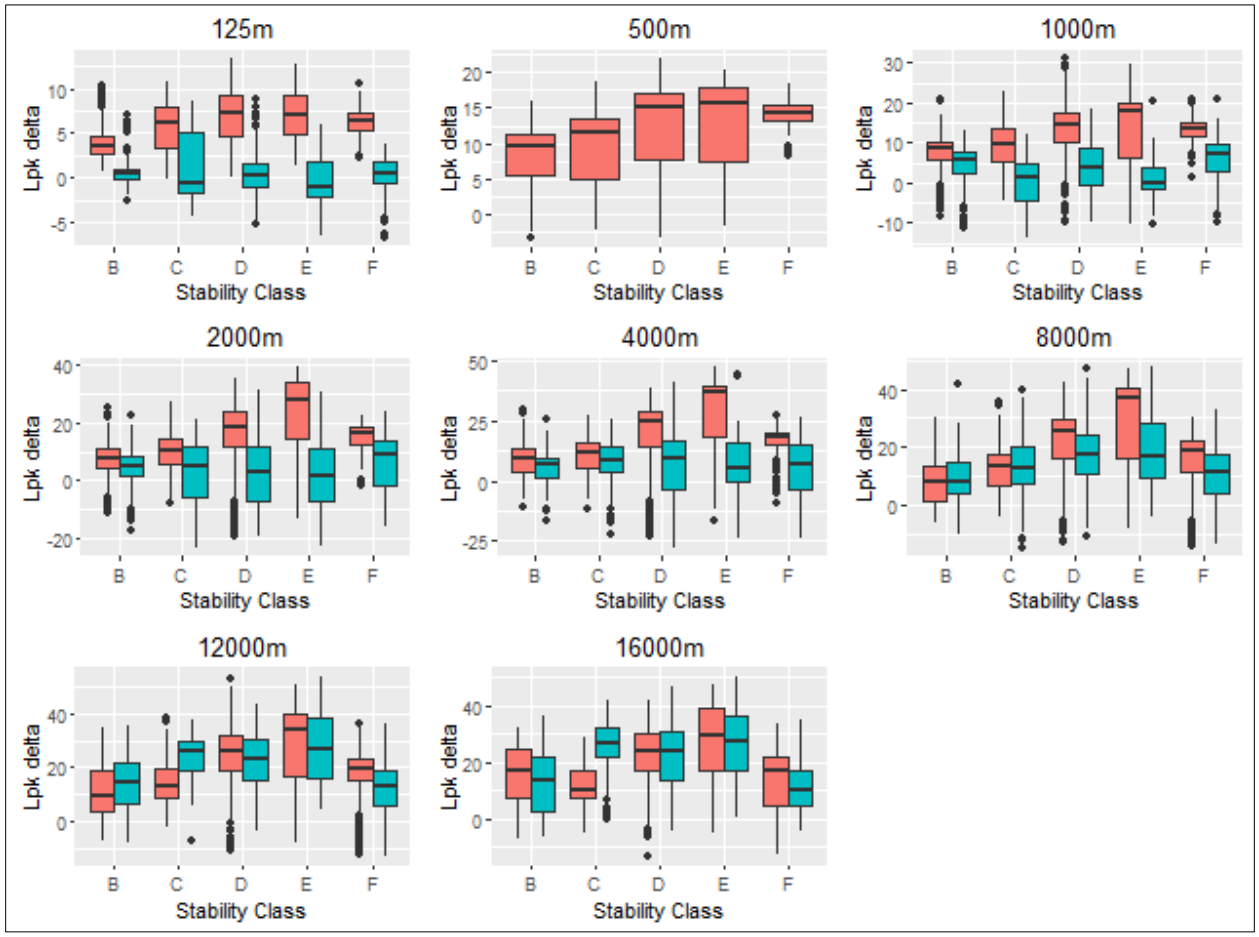

The hexbin plot (Lewin-Koh 2011) below in Figure 10 is a general representation of delta values compared to the expected Lpk values. The color of the hexbins represents number of observations. In general, the higher the Lpk value is expected to be, the better it fit the experiment data.

Figure 10. Hexbin plot representing delta values compared to expected Lpk values.

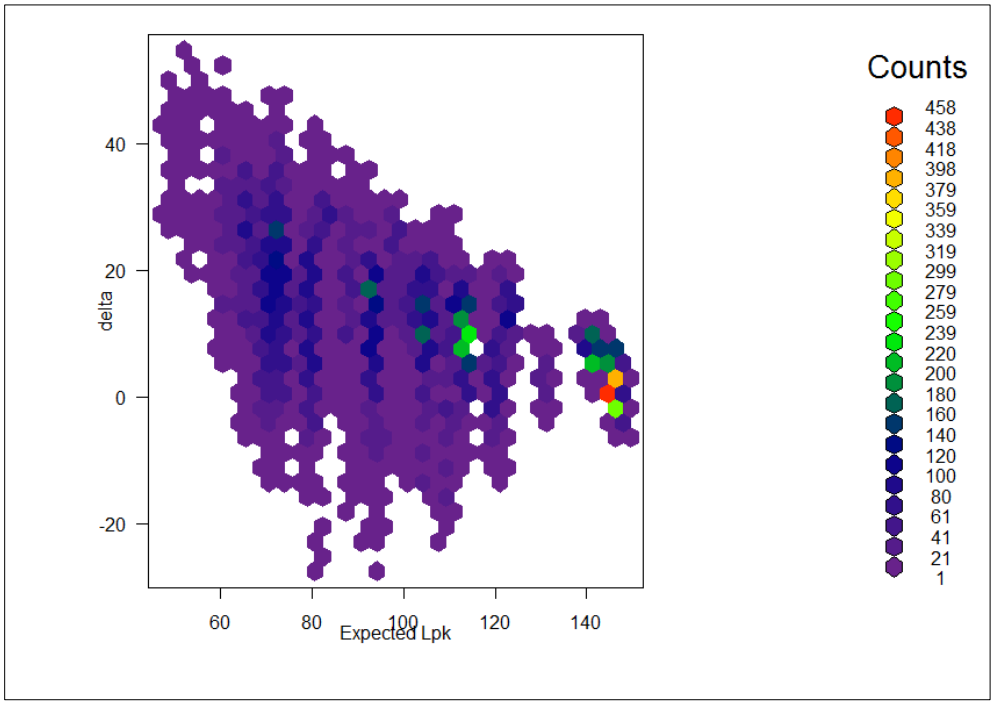

3.4 Summary of results

In summary, the model is underpredicting the measured values approximately 62% of the time overall, with varying percentages under divisions of data. In general, the underpredictions are stronger in the desert environment than in the temperate environment. Additionally, the distributions of residuals are skewed, indicating a potential empirical offset factor present within the calculation engine. The mean underprediction differences were ~12 dB for Lpk values, 7.7 dB for CSEL, and 6.5 for SEL. The code base is being examined closely to identify where this offset is applied and to determine the best method of correction. In addition, the benchmark dataset is being re-investigated in isolation from the noise assessment calculations to determine if there is, perhaps, a more robust manner for calculating a set of propagation conditions.

4 Peak-Level Calculation Algorithms

Because single-event noise assessments often are performed using peak levels (L_{pk}), an evaluation of the peak level estimator was performed. Additionally, three other potential methods were evaluated to determine if there was a more robust or more accurate method to use. The assessment of peak level algorithms is below.

4.1 Assessment of methods for estimating blast peak sound level from energy spectra

In linear propagation models, such as those underlying the noise assessment tools BNoise2 and SARNAM, waveforms are decomposed and propagated according to their frequency components, often in the form of fractional octave band energy spectra. From such Fourier magnitude representations, the overall and weighted sound exposure levels may be reasonably obtained by Riemann sums of the individual bands. However, the peak sound pressure level, L_{pk}, a metric of principal importance for perception, cannot be found in the same way. L_{pk} depends on the *shape* of the waveform in the time domain, which in turn depends on the phase relationship between Fourier components.

Instead of attempting to model the phase propagation from a Fourier transform, a particular waveform shape is selected based on the physical source mechanism. Propagation is then assumed only to scale the source waveform, so that similarity holds at all receiver points. In this way, an implicit phase relationship is *imposed* on the spectral result of the propagation model, which may then be used to infer the peak level.

In this report, several methods for this type of inference are presented, including the mean bandwidth method currently used in the ERDC-CERL noise assessment tools (e.g., BNoise, SARNAM). The ERDC Long-Range Sound Propagation Dataset is then used to test each method, by predicting the peak level from the measured one-third-octave band spectra and comparing it with the actual value. From these residuals, the various estimation methods are compared.

4.2 Energy spectra of a similar waveform

The relationship between a finite-band spectrum and the time-domain waveform can be non-intuitive, especially when the effects of bandwidth are considered. The interrelation between these functions is now derived.

4.2.1 Arbitrary band shape

The Fourier transform of the sound pressure time waveform $p(t)$ is defined as

$$\hat{p}(\omega) = \int_{-\infty}^{\infty} p(t)\, e^{-i\omega t}\, dt, \tag{5}$$

where ω is the angular frequency, which is related to the cyclic frequency f as $\omega = 2\pi f$. For a given band of arbitrary shape implemented as a filter with transfer function $H_i(\omega)$, the band sound exposure E_i is given by

$$E_i = \int_{-\infty}^{\infty} |H_i(\omega)|^2\, |\hat{p}(\omega)|^2\, d\omega = 2\int_{0}^{\infty} |H_i(\omega)|^2\, |\hat{p}(\omega)|^2\, d\omega. \tag{6}$$

Assuming that the sound pressure waveform scales in amplitude with the peak level, p_k, and in time with the inverse of a positive phase duration, t_{pos}, such that

$$p\left(t; p_{\text{pk}}, t_{\text{pos}}\right) = p_{\text{pk}} g\left(\frac{t}{t_{\text{pos}}}\right). \tag{7}$$

From the scale property of the Fourier transform,

$$\hat{p}\left(\omega; p_{\text{pk}}, t_{\text{pos}}\right) = p_{\text{pk}} t_{\text{pos}} \hat{g}(\omega t_{\text{pos}}), \tag{8}$$

where $\hat{g}(\omega)$ is the Fourier transform of the function $g(\tau)$. The magnitude squared then is

$$\left|\hat{p}\left(\omega; p_{\text{pk}}, t_{\text{pos}}\right)\right|^2 = p_{\text{pk}}^2 t_{\text{pos}}^2 \left|\hat{g}\left(\omega t_{\text{pos}}\right)\right|^2. \tag{9}$$

Therefore, the band sound exposure is

$$E_i = 2p_{\text{pk}}^2 t_{\text{pos}} \int_{0}^{\infty} |H_i(\omega)|^2 \left|\hat{g}\left(\omega t_{\text{pos}}\right)\right|^2 t_{\text{pos}}\, d\omega. \tag{10}$$

The band sound exposure level (SEL) is defined by

$$L_{E,i} = 10\log_{10}\left(\frac{E_i}{E_{\text{ref}}}\right), \tag{11}$$

Where $E_{\text{ref}} = p_{\text{ref}}^2 t_{\text{ref}} = 4 \times 10^{-10}$ Pa$^2 \cdot$ s, and $t_{\text{ref}} = 1$ s, so

$$L_{E,i} = 10\log_{10} 2 + 10\log_{10} p_k^2 + 10\log_{10} t_{\text{pos}} + 10\log_{10}\left\{\int_0^\infty |H_i(\omega)|^2 \left|\hat{g}\left(\omega t_{\text{pos}}\right)\right|^2 t_{\text{pos}}\, d\omega\right\} - 10\log_{10} E_{\text{ref}}. \tag{12}$$

Finally, the peak sound pressure level is defined as

$$L_{\text{pk}} = 10\log_{10}\left(\frac{p_{\text{pk}}^2}{p_{\text{ref}}^2}\right), \tag{13}$$

so that the band sound exposure level becomes

$$L_{E,i} = L_{\text{pk}} + 10\log_{10}\left(\frac{t_{\text{pos}}}{t_{\text{ref}}}\right) + 10\log_{10}\left\{\int_0^\infty |H_i(\omega)|^2 \left|\hat{g}\left(\omega t_{\text{pos}}\right)\right|^2 t_{\text{pos}}\, d\omega\right\} + 3. \tag{14}$$

4.2.2 Ideal filter with arbitrary band

If the band filter is idealized as perfect passband between cyclic frequencies $f_{1,i}$ and $f_{2,i}$, then the sound exposure level becomes

$$L_{E,i} = L_{\text{pk}} + 10\log_{10}\left(\frac{t_{\text{pos}}}{t_{\text{ref}}}\right) + 10\log_{10}\left\{\int_{2\pi f_{1,i}}^{2\pi f_{2,i}} \left|\hat{g}\left(\omega t_{\text{pos}}\right)\right|^2 t_{\text{pos}}\, d\omega\right\} + 3, \tag{15}$$

which with the substitution $u = \omega t_{\text{pos}}$ becomes

$$L_{E,i} = L_{\text{pk}} + 10\log_{10}\left(\frac{t_{\text{pos}}}{t_{\text{ref}}}\right) + 10\log_{10}\left\{\int_{2\pi f_{1,i} t_{\text{pos}}}^{2\pi f_{2,i} t_{\text{pos}}} |\hat{g}(u)|^2\, du\right\} + 3. \tag{16}$$

The integral expression can often be evaluated exactly for common waveforms. One example is that of the Friedlander waveform, which is often used to model blast waves. The time-domain pressure function is

$$p(t) = p_{\text{pk}} \begin{cases} 0, t < 0 \\ \left(1 - t/t_{\text{pos}}\right) e^{-t/t_{\text{pos}}}, t \geq 0 \end{cases} \tag{17}$$

so that the similarity function $g(\tau)$ clearly is

$$g(\tau) = \begin{cases} 0, \tau < 0 \\ (1-\tau)\, e^{-\tau}, \tau \geq 0 \end{cases} \tag{18}$$

with Fourier transform

$$\hat{g}(\omega) = \frac{i\omega t_{\text{pos}}}{\left(1+i\omega t_{\text{pos}}\right)^2}. \tag{19}$$

In this case, the integral in the band SEL expression becomes

$$\int_{2\pi f_{1,i} t_{\text{pos}}}^{2\pi f_{2,i} t_{\text{pos}}} |\hat{g}(u)|^2 \, du = \int_{2\pi f_{1,i} t_{\text{pos}}}^{2\pi f_{2,i} t_{\text{pos}}} \frac{u^2}{(1+u^2)^2} \, du. \tag{20}$$

For the Friedlander blast waveform, the sound exposure level in the i^{th} band is given by

$$\begin{aligned} L_{E,i} &= L_{\text{pk}} + 10 \log_{10} \left(\frac{t_{\text{pos}}}{t_{\text{ref}}} \right) \\ &+ 10 \log_{10} \left\{ \begin{matrix} -\frac{2\pi f_{2,i} t_{\text{pos}}}{1+\left(2\pi f_{2,i} t_{\text{pos}}\right)^2} + \tan^{-1}\left(2\pi f_{2,i} t_{\text{pos}}\right) \\ +\frac{2\pi f_{1,i} t_{\text{pos}}}{1+\left(2\pi f_{1,i} t_{\text{pos}}\right)^2} - \tan^{-1}\left(2\pi f_{1,i} t_{\text{pos}}\right) \end{matrix} \right\}. \end{aligned} \tag{21}$$

4.2.3 Effects of band edge frequency ratio

One consequence of the choice of particular band edge frequencies in composing a spectrum is the actual shape obtained. The contrast is greatest between linear and fractional-octave band spectra, where the dimensional slope of the spectrum against a logarithmically-scaled abscissa can change. Consider Figure 11 for example, where two SEL spectra for the same Friedlander waveform with $L_{\text{pk}} = 120$ dB and $t_{\text{pos}} = 30$ ms are shown. Both spectra span the same frequencies with the same number of bands, but each appears completely different. The linearly-spaced bands completely fail to capture the low-frequency transition, and at high frequencies, the dimensional slope is obviously steeper in the linear case. This result highlights the importance of modeling the actual filter bank implementation of the SEL spectra.

Figure 11. Demonstration of the effect of band edge frequency ratio on sound pressure level spectra.

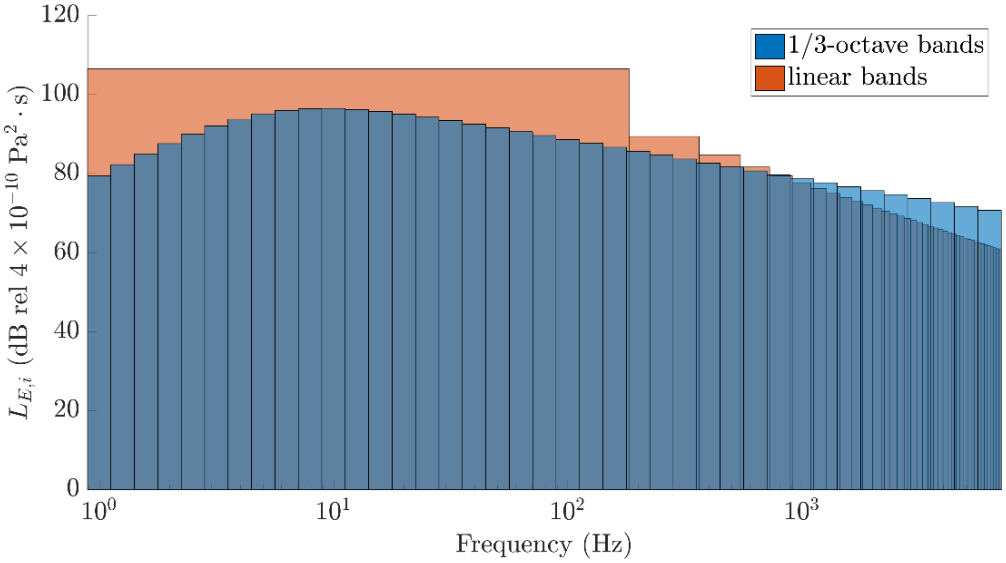

4.3 Methods for peak level estimation

In this report, four methods are considered for estimating the peak pressure level of a blast, based on its fractional octave band spectrum. Three of these methods use the previous formula for the band SEL of a Friedlander waveform. The fourth is the current method employed in the ERDC-CERL noise assessment toolbox, developed by White (2002), which will be presented first.

4.3.1 Mean bandwidth method

The method developed by White (2002) exploits the Schwarz inequality for the mean duration and bandwidth—Δt and Δf, respectively—of a waveform, which requires that

$$\Delta t \Delta f \geq \frac{1}{4\pi}. \tag{22}$$

Both quantities are defined as the ratio of the second central moment of the mean-square pressure to the zeroth central moment, with the difference being that Δt is defined in terms of the time-domain pressure waveform, and Δf is defined from its Fourier transform.

In general, the result is that

$$L_{\mathrm{pk}} = L_E + 10 \log_{10} \left(\frac{\Delta f}{f_0} \right) + \text{const.}, \tag{23}$$

where $f_0 = 1$ Hz. The empirical constant in the expression was determined from an extensive set of small arms muzzle blast and bow shock data, and is different for either case. Here, only the 3 dB empirical offset for muzzle blasts is considered, since they are modeled as the Friedlander waveform.

It is worth noting that in White's (2002) original method, the mean duration Δt is related to the positive phase duration t_{pos} by a waveform-dependent multiplicative constant. Under the assumption that $\Delta t \Delta f = \text{const.}$, this expression becomes essentially identical to that derived for $L_{E,i}$.

4.3.2 Least-squares fitting method

With the expression for $L_{E,i}$, a least-squares fit to the measured spectrum can be performed in the model parameters L_{pk} and t_{pos}. The solution can be obtained immediately in the peak level, since it is a linear term, so that the problem reduces to a one-dimensional zero-finding problem.

This approach is very sensitive to the shape of the spectrum that is fit, and the approach cannot be expected to perform well when the actual waveform is not as well-approximated as Friedlander. For example, Figure 12 shows the best fit failing to capture the amplitude of the broadband peak. One could expect an under-prediction of L_{pk} in this case.

Figure 12. Example of a least-squares fit of the Friedlander result to a measured one-third-octave band spectrum.

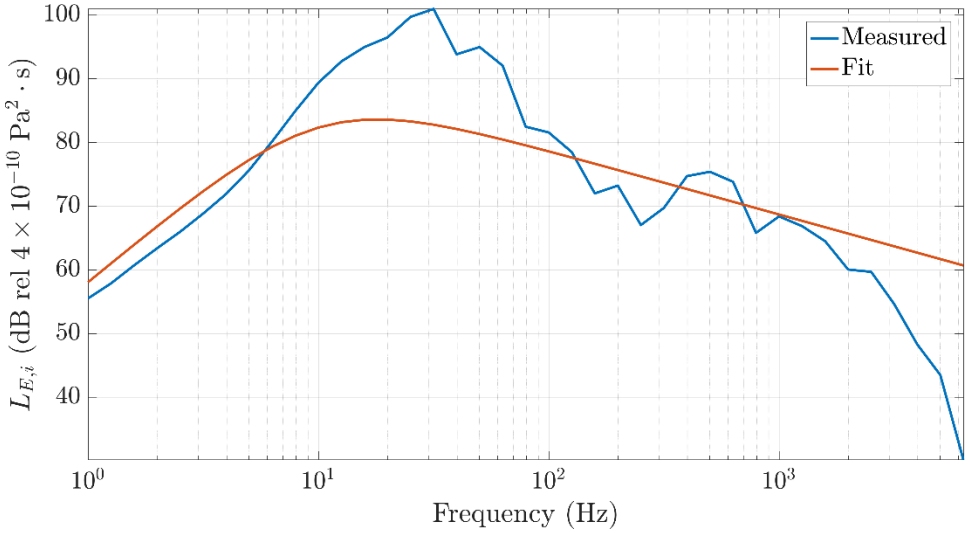

4.3.3 Hybrid L_E-t_{pos} method

It is also possible to ignore the value obtained by fitting L_{pk}, and use the estimated overall SEL instead. This approach was motivated by the poor performance of the previous. The overall SEL is defined in terms of the integral of the square Fourier pressure over all frequencies, i.e.,

$$L_E = 10 \log_{10} \left(\frac{\int_{-\infty}^{\infty} |\hat{p}(\omega)|^2 \, d\omega}{E_{\text{ref}}} \right). \tag{24}$$

For the Friedlander waveform, this integral evaluates to

$$\int_{-\infty}^{\infty} |\hat{p}(\omega)|^2 \, d\omega = 2 p_{\text{pk}}^2 t_{\text{pos}} \int_0^{\infty} \frac{u^2}{(1+u^2)^2} \, du = \frac{\pi}{2} p_{\text{pk}}^2 t_{\text{pos}}, \tag{25}$$

and so the overall sound exposure level is

$$L_E = 10 \log_{10} \left(\frac{\frac{\pi}{2} p_k^2 t_{\text{pos}}}{E_{\text{ref}}} \right) = L_{\text{pk}} + 10 \log_{10} \left(\frac{t_{\text{pos}}}{t_{\text{ref}}} \right) + 2, \tag{26}$$

which is equivalent to the equation for $L_{E,i}$ for $f_{1,i} = 0$ in the limit as the band becomes infinitely wide. This equation solved for the peak pressure level is

$$L_{\text{pk}} = L_E - 10 \log_{10} \left(\frac{t_{\text{pos}}}{t_{\text{ref}}} \right) - 2, \tag{27}$$

and therefore the peak level may be found from the unweighted sound exposure level and the positive phase duration estimate.

4.3.4 Peak frequency method

With the previous formula, it is also possible to estimate the positive phase duration from the peak band in the one-third-octave band spectrum, according to

$$t_{\text{pos}} \approx \frac{1}{2\pi f_{\max}}, \tag{28}$$

$$\text{so that } L_{\text{pk}} = L_E + 10\log_{10}(f_{\max} t_{\text{ref}}) - 10. \tag{29}$$

4.4 ERDC Long-Range Sound Propagation Dataset analysis

The ERDC Long-Range Sound Propagation Dataset of acoustic blast waveforms was used to compare the four methods for peak level estimation. Each blast measurement was used in the analysis, with the exception of those recorded by the blast pencils, which were very near to the source and showed different scaling than the scaling observed by the microphone array at range. A total of 13,133 blast measurements were analyzed. For each, the measured L_{pk}, L_E, and one-third-octave band spectra were available. The latter two metrics were used to estimate the former with all four methods, and then compared with the observed value as residuals according to

$$\Delta \text{L}_{\text{pk}} = L_{\text{pk,obs}} - L_{\text{pk,est}}. \tag{30}$$

4.4.1 Comparison of estimation methods

Figure 13 shows histograms of the residuals for each of the peak level estimation methods. In terms of average performance, it is evident that the L_E-t_{pos} estimator is best, with a 1–2 dB average underprediction. The direct least-squares fitting method underpredicts the peak level in almost all cases, with up to a 20 dB deficit observed, while the mean bandwidth and L_E-$f_{\max}$ estimators overpredict by the same amount, on average.

Figure 13. Histograms of the residuals for each peak level estimator.

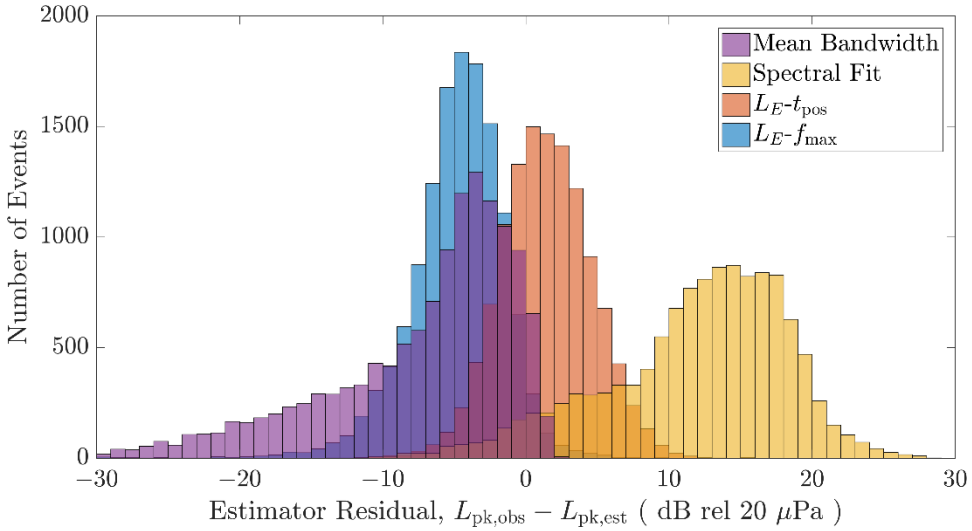

The distributions of each estimator are also noteworthy. It is clear that the hybrid L_E-t_{pos} and L_E-f_{max} estimators yield low-skewness nearly-normal distributions, especially the former estimator. The direct fitting method gives a broad, heavy-tailed distribution. Most importantly, while the mean bandwidth estimator has similar average performance to the L_E-f_{max} estimator, its residual distribution has a heavy tail toward overprediction, which is an undesirable property.

However, these distributions improve if limited to comparisons with blast measurements with peak levels over 100 dB, as seen in Figure 14. The direct fitting estimator is still broadly distributed compared with the other estimators, but the heavy tail in the mean-bandwidth estimator is no longer present. A similar, although not as effective, result is obtained when the dataset is restricted to measurements within 12 km of the source, as shown in Figure 15.

An important caveat to the improved performance of the L_E-t_{pos} estimator is the sensitivity to the starting point of the curve fit for t_{pos}. If a poor starting point is chosen, the least-squares fit is not guaranteed to converge, especially when the spectrum has features not associated with the Friedlander waveform. The best starting point seems to be near the estimate of t_{pos} given by f_{max}. In fact, this realization was how the peak frequency method was developed. A more robust fitting method must be developed if the L_E-t_{pos} estimator is to be implemented in the noise assessment tools.

Figure 14. Histograms of the residuals for each peak level estimator for events with peak level over 100 dB.

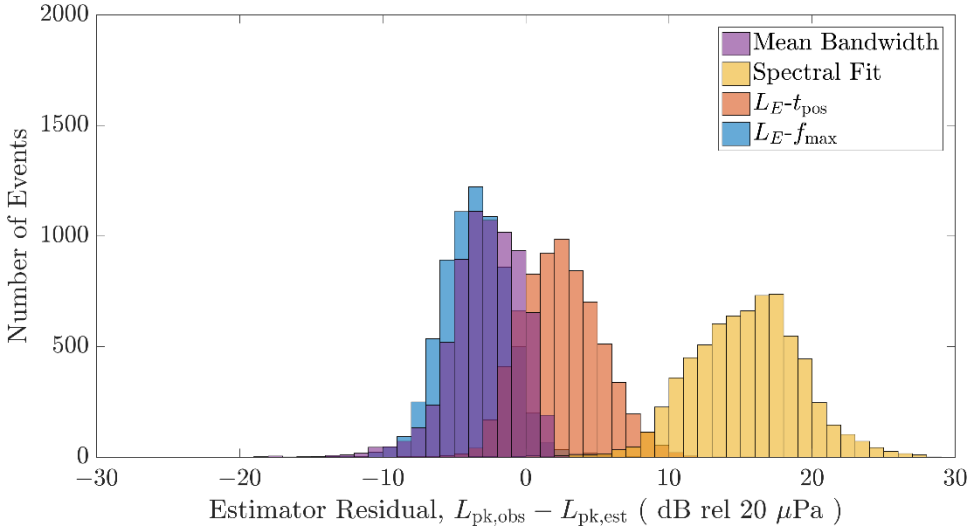

Figure 15. Histograms of the residuals for each peak level estimator for events within 12 km of the source.

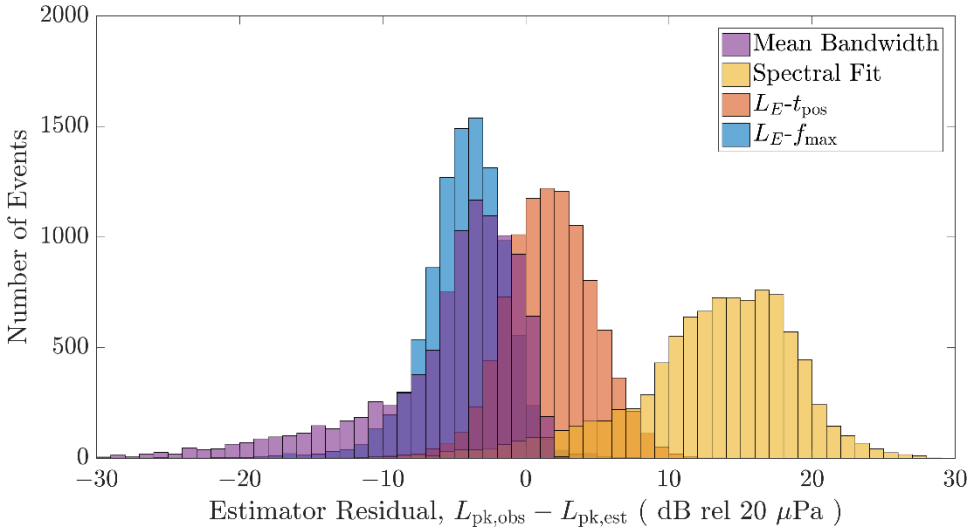

4.4.2 Analysis of the mean bandwidth method

Since it is the method currently implemented in the noise assessment toolbox, the mean bandwidth estimator was analyzed further. First, consider the effect of restricting the set of blast events by peak pressure level, shown in Figure 16. As the peak threshold is increased, the heavy over-predictive tail of the estimator residuals is removed, improving the result. This can be explained by the fact that the structure in the Friedlander waveform is physically more representative of a waveform with great enough overpressure to sustain a weak shock front. For weaker peak levels, the Friedlander blast waveform is less appropriate.

Figure 16. Histograms of the residuals for the mean bandwidth estimator, restricted by peak level threshold.

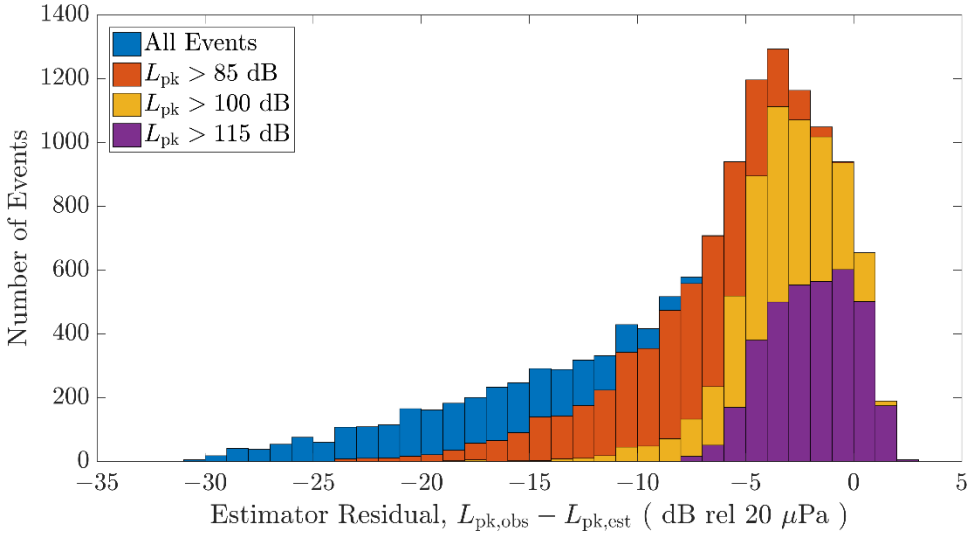

The effect of restricting the range of observed blasts is different, as seen in Figure 17. Note that as the range limit moves nearer to the source, the entire distribution is scaled and the heavy tail is largely retained. This suggests that the over-prediction is principally an effect of overpressure magnitude, not propagation.

Figure 17. Histograms of the residuals for the mean bandwidth estimator, restricted by propagation range.

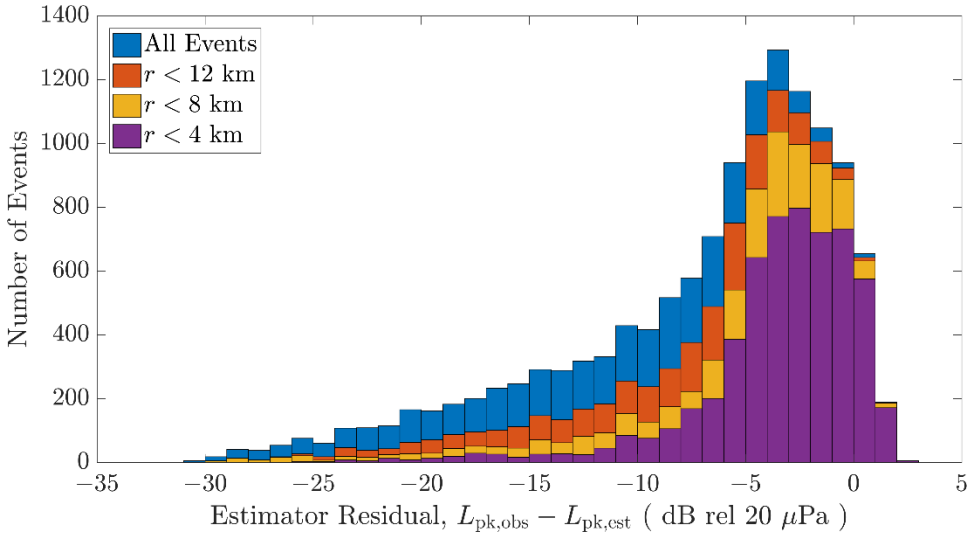

Finally, consider the scatterplot in Figure 18, made in the same way as similar plots by White (2002). The mean bandwidth method ideally would show all the points collapsing along the dashed line. Clearly, this is not the

case, but the L_{pk} colormap demonstrates what has already been observed in the histograms: the estimator improves with increasing peak level.

Figure 18. Scatterplot of the overall SEL difference from the peak level against mean bandwidth.

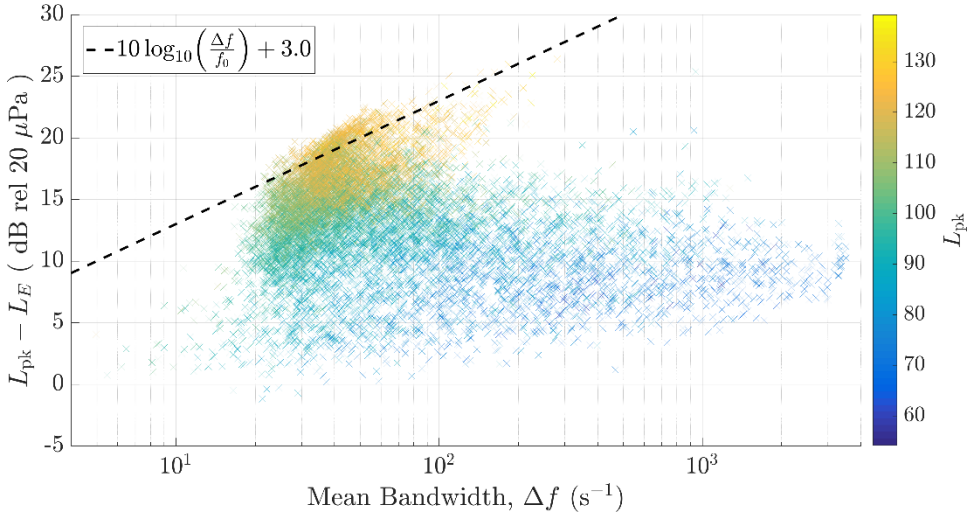

4.5 Conclusions

The hybrid L_E-t_{pos} estimator developed in this report for the peak sound pressure level from the one-third-octave band spectrum has outperformed the current mean bandwidth estimator. On average, the L_E-f_{max} estimator performs at least as well as the mean bandwidth. The residuals for both of these estimators exhibit less deviation and skewness than the mean bandwidth estimator. The residual distribution of the mean bandwidth estimator improves when only blasts with peak levels greater than 100 dB are considered, although a small mean offset is still apparent.

4.6 Recommendations

Two potential courses of action are recommended for improving the peak level estimation method within the noise assessment tools:

1. A more robust fitting method for the hybrid L_E-t_{pos} estimator can be developed to permit its implementation. Considerations would be necessary for handling arbitrarily shaped spectra and rejecting the Friedlander waveform hypothesis; then, both the mean performance and estimator distribution would be improved.

2. An empirical offset can be introduced to the L_E-$f_{\max}$ estimator to bring its mean residual to zero. There could be unforeseen issues in estimating $f_{\max}$ for arbitrarily shaped spectra. However, the estimator distribution would be improved, and no curve fitting would be necessary.

5 Meteorological Conditions and Propagation Classification

The results of short-term noise assessment calculations are directly dependent upon the acoustic propagation class selected. These propagation classes are based upon averaged meteorological conditions. The set of propagation classes is designed to encompass those meteorological conditions that are most likely to occur regularly across the continental United States (CONUS).

Two major items were investigated in this portion of the project. First, an analysis was performed of the variability of meteorological conditions and their associated mapping to generalized acoustic propagation classes. The goal was to determine how variable the meteorological measurements were across the landscape during the ERDC Long-Range Sound Propagation experiment (Valente et al. 2012b). This variability is an indicator of how much error could be introduced due to the assumption that the propagation condition is the same for the entire area. If the result was that the variability was minimal, an added benefit would be the inclusion of additional acoustic data in the statistical analysis. A subset of data was discarded from the statistical analysis described in Section 3 due to equipment failures on meteorological towers. The second task investigated the accuracy of the "quick" selection tool currently utilized by the RMTK Noise Tool for choosing the correct propagation class for a noise assessment. This selection tool is based on the statistically most-likely-to-occur condition from a climatological perspective, based on time of day, season, ground type (grass or desert), wind speed, wind direction, and cloud cover. Both of these tasks and their results are described in this section.

5.1 Variability of propagation conditions across the landscape

The ERDC Long-Range Sound Propagation experiment utilized 15-meter high instrumented meteorological towers to sample the atmospheric boundary layer conditions during the tests. One tower was placed approximately midway along each of the three acoustic propagation directions sampled. The propagation classes derived from the meteorological conditions at the time of each detonation are synchronized with the acoustic data by propagation direction. This synchronization means that if sensors failed on one tower and not enough information was available to determine the propagation classification, data along that propagation line is

discarded from the analysis set for all of those occurrences that do not have a correlating propagation condition. A study of the meteorological data was performed to determine how much variability was present across the measurement landscape, an area within a 16 km radius surrounding a central point.

Four data-collection periods are considered: desert summer (NM07), desert winter (NM08), temperate summer (MO08) and temperate winter (MO09). Four towers were set up during these periods—other than NM07, where only three towers were available. The towers were located as follows: one to each of the three propagation lines and one near the center of the array for all except NM07. Data from each tower was processed into a Pasquill stability class and wind speed; these classifications were then compared across the towers for each time stamp. Classifications were derived from temperature data at 1 m and 10 m heights and from wind speed at 10 m height, using the Solar Radiation Delta-T (SRD-T) method (Coulter 1993). Tower C during NM07 did not have a working temperature sensor at 10 m height, so the 6 m sensor was used instead. Values of incoming solar radiation were used at each tower as well. The schematic for selecting a Pasquill stability class (Pasquill 1974) is shown in Table 5.

Table 5. Definitions of the SRD-T method for estimating Pasquill-Gifford (P-G) stability categories, A–D for daytime and D–F for nighttime.

Daytime				
Wind Speed (m/sec)	Solar Radiation (W/m²)			
	≥ 925	925–675	675–175	< 175
< 2	A	A	B	D
2–3	A	B	C	D
3–5	B	B	C	D
5–6	C	C	D	D
≥ 6	C	D	D	D
Nighttime				
Wind Speed (m/s)	Vertical Temperature Gradient			
	< 0		> 0	
< 2.0	E		F	
2.0–2.5	D		E	
≥ 2.5	D		D	

The comparison results for each time period (compared by timestamp) are shown in Figure 19–Figure 22. The worst case was NM07, where the three towers matched only 36% of the time. The other three measurement periods had all four towers match stability class approximately 50% of the time (53% for NM08, 52% for M008, and 50% for MO09).

Figure 19. Relative frequency of occurrence of stability class, NM07.

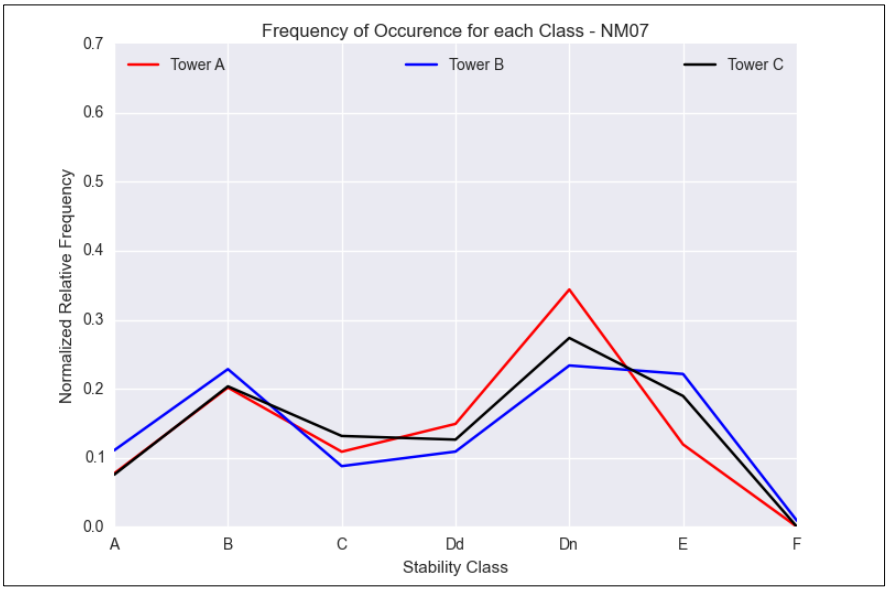

Figure 20. Relative frequency of occurrence of stability class, NM08.

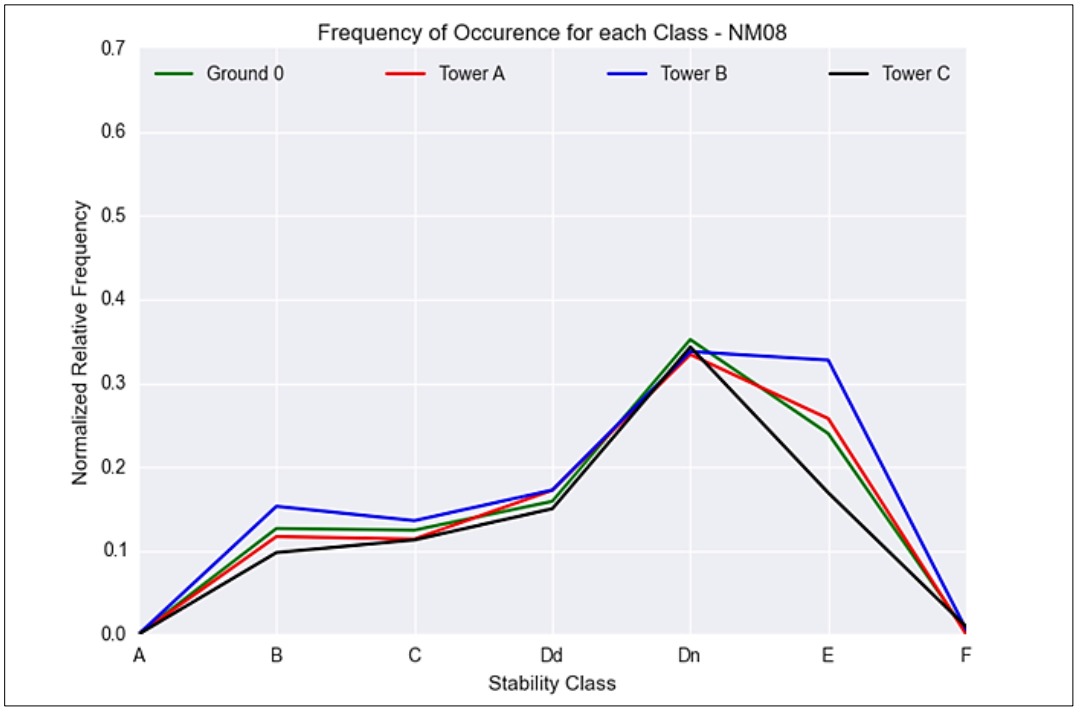

Figure 21. Relative frequency of occurrence of stability class, MO08.

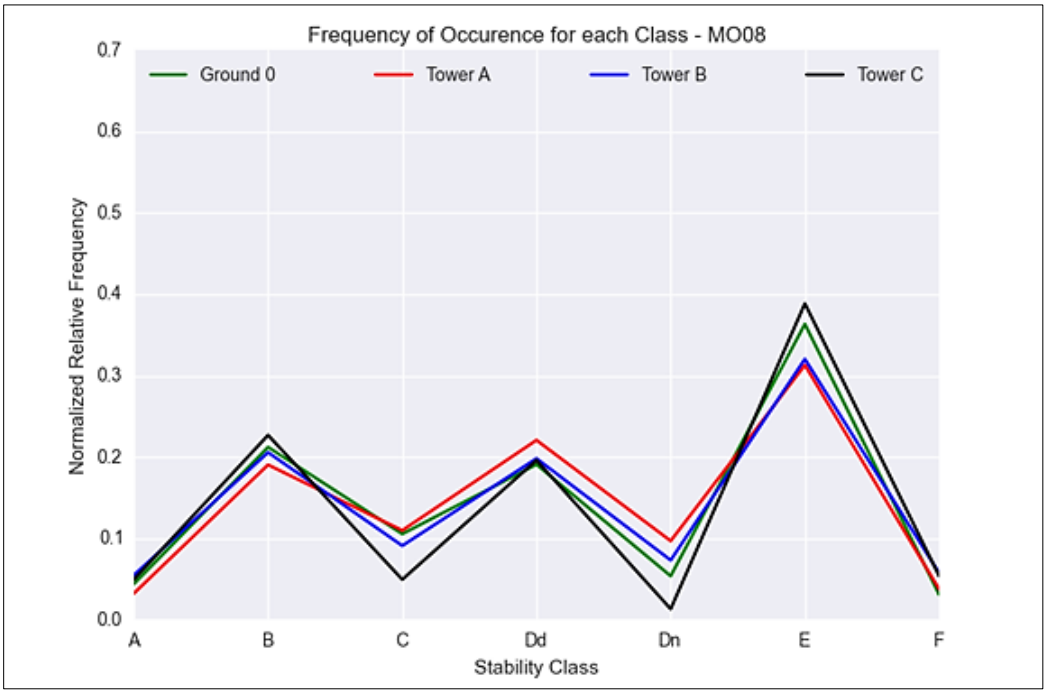

Figure 22. Relative frequency of occurrence of stability class, MO09.

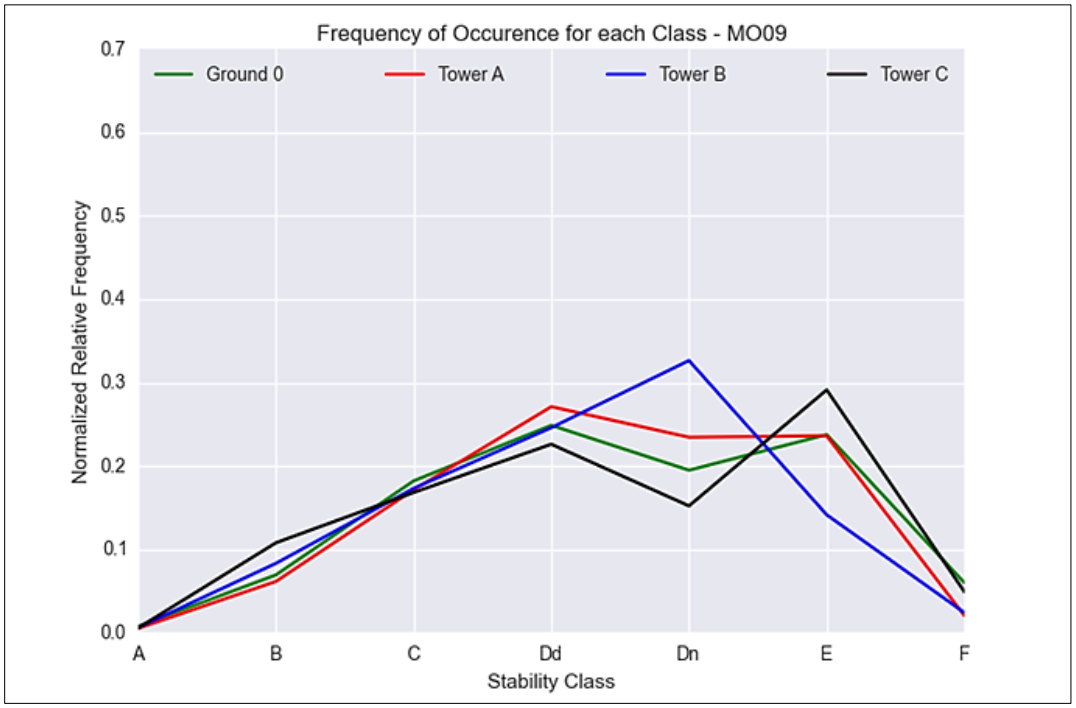

Since, at best, the stability class across all towers for the same timestamp matches only 53% of the time, it cannot said with confidence that a point measurement will yield the correct stability class across a region. However, in reality, a user will often have access to only one meteorological station.

Investigations into whether a nearby weather station yields comparable results are ongoing. Other options for determining the propagation class are also being investigated and will be described in a future report.

5.2 Propagation class selection tool

The RMTK Noise Tool currently uses a quick selection tool as a method for determine the appropriate propagation tables to use for a calculation. This selection tool asks the user to input simple, easily obtained information. RMTK selects appropriate propagation tables for that case. The parameters are time of day, season, cloud cover, wind speed, wind direction, and ground type. These mappings are based on the propagation class most likely to occur in a climatological statistical manner for the entire continental United States. The mappings were based on data from seven geographically-dispersed locations. There was little variation in the most common condition across these locations, so a common set was defined for grass (temperate) and desert locations.

Estimator tables depend upon both a season and a day or night designation. Therefore, comparisons between the mapping tables and the recorded data are divided in that same manner. Since the two temperate location datasets were collected near the transition between seasons (late summer/early fall, late winter/early spring), comparisons are made to both seasons. In each set of comparative tables, the generalized estimator is displayed first, followed by a table of percentage of occurrences and a table of number of occurrences. Both percentage of occurrence and number of occurrences are important, since there are conditions that only occurred a small number of times. Data for cloud cover was obtained from Automated Surface Observing Station (ASOS) observations at the nearest weather station. This provides consistency between day and night mappings because the meteorological towers relied on solar radiation sensors to estimate cloud cover and had no method at all for determining cloud cover during the night.

5.2.1 NM07 (summer day, desert)

The estimator (Table 6) accurately predicted the most likely condition in 7 of the 10 conditions measured (Table 7). Note that there were no mostly cloudy or overcast days that occurred during the measurement period (Table 8).

Table 6. Estimator for summer day – desert.

Cloud Amount	Wind Speed (kn)				
	0	1–5	6–10	11–15	>=16
Clear	B	B	C	D	D
Partly Cloudy	B	B	C	D	D
Mostly Cloudy	D	C	C	D	D
Overcast	D	D	D	D	D

Table 7. Percentage occurrence of Pasquill stability classes from measurements, summer day – desert.

Cloud Amount	Wind Speed (kn)				
	0	1–5	6–10	11–15	>=16
Clear	A: 0% B: 66.7% C: 4% D: 29.3%	A: 16% B: 54% C: 17.8% D: 12.2%	A: 14.7% B: 49.1% C: 30.2% D: 6.1%	A: 6.1% B: 27.8% C: 33% D: 33%	A: 0% B: 0% C: 0% D: 100%
Partly Cloudy	A: 22.5% B: 54.1% C: 8.6% D: 14.7%	A: 22.9% B: 51.4% C: 14.2% D: 11.5%	A: 16.8% B: 51.8% C: 23.1% D: 8.2%	A: 7.7% B: 30.7% C: 20.7% D: 40.8%	A: 0% B: 1.4% C: 2.9% D: 95.7%
Mostly Cloudy	N/A	N/A	N/A	N/A	N/A
Overcast	N/A	N/A	N/A	N/A	N/A

Table 8. Frequency of occurrence of Pasquill stability classes from measurements, summer day – desert.

Cloud Amount	Wind Speed (kn)				
	0	1–5	6–10	11–15	>=16
Clear	A: 0 B: 50 C: 3 D: 22	A: 491 B: 1662 C: 548 D: 376	A: 228 B: 763 C: 469 D: 95	A: 7 B: 32 C: 38 D: 38	A: 0 B: 0 C: 0 D: 15
Partly Cloudy	A: 250 B: 602 C: 96 D: 164	A: 2321 B: 5217 C: 1437 D: 1166	A: 1040 B: 3208 C: 1433 D: 510	A: 104 B: 413 C: 278 D: 549	A: 0 B: 2 C: 4 D: 133
Mostly Cloudy	N/A	N/A	N/A	N/A	N/A
Overcast	N/A	N/A	N/A	N/A	N/A

5.2.2 NM07 (summer night, desert)

The estimator (Table 9) accurately predicted the most likely condition in 6 of the 14 conditions measured (Table 10). Note that not all conditions occurred during the measurement period (Table 11).

Table 9. Estimator for summer night – desert.

	Wind Speed (kn)				
Cloud Amount	0	1–5	6–10	11–15	>=16
Clear	F	F	E	D	D
Partly Cloudy	F	F	E	D	D
Mostly Cloudy	E	D	D	D	D
Overcast	D	D	D	D	D

Table 10. Percentage occurrence of Pasquill stability classes from measurements, summer night – desert.

	Wind Speed (kn)				
Cloud Amount	0	1–5	6–10	11–15	>=16
Clear	D: 26.6% E: 73.2% F: 0.2%	D: 48.8% E: 49.5% F: 1.6%	D: 72.8% E: 26.3% F: 0.8%	D: 97.6% E: 1.9% F: 0.5%	D: 100% E: 0% F: 0%
Partly Cloudy	D: 50.1% E 39.7% F: 10.2%	D: 55.7% E: 36.7% F: 7.6%	D: 80% E: 14.9% F: 5.1%	D: 91% E: 7.2% F: 1.7%	N/A
Mostly Cloudy	N/A	D: 50.3% E: 49.7% F: 0%	D: 59.6% E: 40.4% F: 0%	N/A	N/A
Overcast	D: 12.5% E: 87.5% F: 0%	D: 26.2% E: 55.7% F: 18.1%	D: 59.2% E: 24.5% F: 16.3%	N/A	N/A

Table 11. Frequency of occurrence of Pasquill stability classes from measurements, summer night – desert.

	Wind Speed (kn)				
Cloud Amount	0	1–5	6–10	11–15	>=16
Clear	D: 406 E: 1,118 F: 3	D: 4,668 E: 4,733 F: 156	D: 3,951 E: 1,430 F: 46	D: 401 E: 8 F: 2	D: 128 E: 0 F: 0
Partly Cloudy	D: 446 E: 353 F: 91	D: 3,174 E: 2,093 F: 431	D: 4,160 E: 777 F: 265	D: 366 E: 29 F: 7	N/A

Cloud Amount	Wind Speed (kn)				
	0	1–5	6–10	11–15	>=16
Mostly Cloudy	N/A	D: 286 E: 283 F: 0	D: 99 E: 67 F: 0	N/A	N/A
Overcast	D: 1 E: 7 F: 0	D: 101 E: 215 F: 70	D: 29 E: 12 F: 8	N/A	N/A

5.2.3 NM08 (winter day, desert)

The estimator (Table 12) accurately predicted the most likely condition in 14 of the 17 conditions measured (Table 13). Note that not all conditions occurred during the measurement period (Table 14).

Table 12. Estimator for winter day – desert.

Cloud Amount	Wind Speed (kn)				
	0	1–5	6–10	11–15	>=16
Clear	B	B	C	D	D
Partly Cloudy	B	C	C	D	D
Mostly Cloudy	D	C	D	D	D
Overcast	D	D	D	D	D

Table 13. Percentage occurrence of Pasquill stability classes from measurements, winter day – desert.

Cloud Amount	Wind Speed (kn)				
	0	1–5	6–10	11–15	>=16
Clear	A: 0% B: 38.5% C: 0% D: 61.5%	A: 0% B: 51% C: 22% D: 27%	A: 0% B: 4.6% C: 77.1% D: 18.4%	A: 0% B: 2.6% C: 8.5% D: 88.9%	A: 0% B: 0% C: 0% D: 100%
Partly Cloudy	A: 0% B: 27.2% C: 0% D: 72.7%	A: 0.1% B: 56.3% C: 23.6% D: 20.1%	A: 0% B: 3.6% C: 74.1% D: 22.2%	A: 0% B: 0% C: 12% D: 88%	N/A
Mostly Cloudy	A: 0% B: 0% C: 0% D: 100%	A: 0% B: 15.8% C: 18.7% D: 65.5%	A: 0% B: 3.1% C: 33.5% D: 63.4%	A: 0% B: 0% C: 7% D: 93%	N/A
Overcast	N/A	A: 0% B: 21.8% C: 8.3% D: 69.9%	A: 0% B: 7.1% C: 9.4% D: 83.5%	A: 0% B: 0% C: 0.9% D: 99.1%	A: 0% B: 0% C: 0% D: 100%

Table 14. Frequency of occurrence of Pasquill stability classes from measurements, winter day – desert

Cloud Amount	Wind Speed (kn)				
	0	1–5	6–10	11–15	>=16
Clear	A: 0 B: 25 C: 0 D: 40	A: 0 B: 680 C: 294 D: 360	A: 0 B: 26 C: 440 D: 105	A: 0 B: 7 C: 23 D: 241	A: 0 B: 0 C: 0 D: 33
Partly Cloudy	A: 0 B: 12 C: 0 D: 32	A: 1 B: 996 C: 417 D: 356	A: 0 B: 32 C: 654 D: 196	A: 0 B: 0 C: 24 D: 176	N/A
Mostly Cloudy	A: 0 B: 0 C: 0 D: 25	A: 0 B: 32 C: 38 D: 133	A: 0 B: 5 C: 54 D: 101	A: 0 B: 0 C: 4 D: 53	N/A
Overcast	N/A	A: 0 B: 29 C: 11 D: 93	A: 0 B: 6 C: 8 D: 71	A: 0 B: 0 C: 1 D: 107	A: 0 B: 0 C: 0 D: 6

5.2.4 NM08 (winter night, desert)

The estimator (Table 15) accurately predicted the most likely condition in 9 of the 16 conditions measured (Table 16). Note that not all conditions occurred during the measurement period (Table 17).

Table 15. Estimator for winter night – desert.

Cloud Amount	Wind Speed (kn)				
	0	1–5	6–10	11–15	>=16
Clear	F	F	E	D	D
Partly Cloudy	F	F	E	D	D
Mostly Cloudy	F	E	D	D	D
Overcast	D	D	D	D	D

Table 16. Percentage occurrence of Pasquill stability classes from measurements, winter night – desert.

Cloud Amount	Wind Speed (kn)				
	0	1–5	6–10	11–15	>=16
Clear	D: 14.8% E: 81.6% F: 3.6%	D: 37.2% E: 59.8% F: 3%	D: 83.9% E: 14.9% F: 1.2%	D: 100% E: 0% F: 0%	N/A
Partly Cloudy	D: 10% E: 86.7% F: 3.3%	D: 50.6% E: 45.6% F: 3.8%	D: 89.3% E: 9% F: 1.7%	D: 100% E: 0% F: 0%	N/A

Cloud Amount	Wind Speed (kn)				
	0	1–5	6–10	11–15	>=16
Mostly Cloudy	D: 21.4% E: 71.4% F: 7.1%	D: 46.7% E: 52.8% F: 0.5%	D: 86.7% E: 12.9% F: 0.3%	D: 100% E: 0% F: 0%	N/A
Overcast	D: 0% E: 100% F: 0%	D: 47.4% E: 52.6% F: 0%	D: 93.8% E: 6.2% F: 0%	D: 100% E: 0% F: 0%	N/A

Table 17: Frequency of occurrence of Pasquill stability classes from measurements, winter night – desert.

Cloud Amount	Wind Speed (kn)				
	0	1–5	6–10	11–15	>=16
Clear	D: 33 E: 182 F: 8	D: 1,305 E: 2,094 F: 15	D: 1,045 E: 185 F: 15	D: 178 E: 0 F: 0	N/A
Partly Cloudy	D: 3 E: 26 F: 1	D: 405 E: 365 F: 30	D: 516 E: 52 F: 10	D: 85 E: 0 F: 0	N/A
Mostly Cloudy	D: 3 E: 10 F: 1	D: 183 E: 207 F: 2	D: 248 E: 37 F: 1	D: 107 E: 0 F: 0	N/A
Overcast	D: 0 E: 3 F: 0	D: 143 E: 159 F: 0	D: 197 E: 13 F: 0	D: 22 E: 0 F: 0	N/A

5.2.5 M008 (summer day, temperate)

The estimator (Table 18) accurately predicted the most likely condition in 8 of the 14 conditions measured (Table 19). Note that not all conditions occurred during the measurement period (

Table 20).

Table 18. Estimator for summer day – temperate.

Cloud Amount	Wind Speed (kn)				
	0	1–5	6–10	11–15	>=16
Clear	B	C	D	D	D
Partly Cloudy	B	C	D	D	D
Mostly Cloudy	D	D	D	D	D
Overcast	D	D	D	D	D

Table 19. Percentage occurrence of Pasquill stability classes from measurements, summer day – temperate.

Cloud Amount	Wind Speed (kn)				
	0	1–5	6–10	11–15	>=16
Clear	A: 0% B: 30.3% C: 3.1% D: 66.6%	A: 8.1% B: 43% C: 14.7% D: 34.2%	A: 4.6% B: 41.9% C: 36.5% D: 16.9%	A: 0% B: 0% C: 37.5% D: 62.5%	N/A
Partly Cloudy	A: 0.6% B: 5.7% C: 0.3% D: 30.8%	A: 13.9% B: 37.4% C: 18% D: 30.8%	A: 7.4% B: 33.9% C: 32.7% D: 26%	N/A	N/A
Mostly Cloudy	A: 0.8% B: 34.2% C: 2.5% D: 62.5%	A: 5.4% B: 36.7% C: 19.1% D: 38.8%	A: 1.7% B: 25% C: 22.5% D: 50.7%	A: 0% B: 0% C: 0% D: 100%	N/A
Overcast	A: 0% B: 0% C: 0% D: 100%	A: 6.4% B: 24.3% C: 12.2% D: 57.1%	A: 2.8% B: 19.4% C: 25% D: 52.1%	N/A	N/A

Table 20. Frequency of occurrence of Pasquill stability classes from measurements, summer day – temperate.

Cloud Amount	Wind Speed (kn)				
	0	1–5	6–10	11–15	>=16
Clear	A: 0 B: 347 C: 36 D: 763	A: 422 B: 2,228 C: 763 D: 1774	A: 40 B: 364 C: 317 D: 147	A: 0 B: 0 C: 3 D: 5	N/A
Partly Cloudy	A: 2 B: 19 C: 1 D: 313	A: 632 B: 1,703 C: 821 D: 1,402	A: 73 B: 336 C: 324 D: 257	N/A	N/A
Mostly Cloudy	A: 1 B: 41 C: 3 D: 75	A: 632 B: 1,703 C: 821 D: 729	A: 11 B: 160 C: 144 D: 324	A: 0 B: 0 C: 0 D: 4	N/A
Overcast	A: 0 B: 0 C: 0 D:20	A: 76 B: 289 C: 145 D: 678	A: 4 B: 28 C: 37 D: 75	N/A	N/A

5.2.6 M008 (summer night, temperate)

The estimator (Table 21) accurately predicted the most likely condition in 9 of the 16 conditions measured (Table 22). Note that not all conditions occurred during the measurement period (Table 23).

Table 21. Estimator for summer night – temperate.

Cloud Amount	Wind Speed (kn)				
	0	1–5	6–10	11–15	>=16
Clear	F	F	D	D	D
Partly Cloudy	F	F	D	D	D
Mostly Cloudy	E	D	D	D	D
Overcast	D	D	D	D	D

Table 22. Percentage occurrence of Pasquill stability classes from measurements, summer night – temperate.

Cloud Amount	Wind Speed (kn)				
	0	1–5	6–10	11–15	>=16
Clear	D: 3.4% E: 94.3% F: 2.4%	D: 6.8% E: 89.3% F: 3.9%	D: 48.3% E: 46.7% F: 5%	D: 91.7% E: 8.3% F: 0%	D: 50% E: 25% F: 25%
Partly Cloudy	D: 3.5% E: 90.8% F: 5.7%	D: 17.9% E: 67.1% F: 14.9%	D: 56% E: 24% F: 20%	N/A	N/A
Mostly Cloudy	D: 5.6% E: 90.6% F: 3.8%	D: 25.6% E: 59.3% F: 15.1%	D: 59.1% E: 21.8% F: 19.1%	D: 75% E: 12.5% F: 21.5%	N/A
Overcast	D: 1.1% E: 96.6% F: 2.3%	D: 22.5% E: 43.6% F: 33.9%	D: 62.5% E: 20.4% F: 17.1%	D: 100% E: 0% F: 0%	N/A

Table 23. Frequency of occurrence of Pasquill stability classes from measurements, summer night – temperate.

Cloud Amount	Wind Speed (kn)				
	0	1–5	6–10	11–15	>=16
Clear	D: 182 E: 5,106 F: 129	D: 443 E: 5,789 F: 254	D: 87 E: 84 F: 9	D: 22 E: 2 F: 0	D: 2 E: 1 F: 1
Partly Cloudy	D: 24 E: 620 F: 39	D: 312 E: 1,169 F: 260	D: 210 E: 90 F: 75	N/A	N/A
Mostly Cloudy	D: 22 E: 355 F: 15	D: 309 E: 715 F: 182	D: 220 E: 81 F: 71	D: 6 E: 1 F: 1	N/A
Overcast	D: 1 E: 85 F: 2	D: 238 E: 460 F: 358	D: 95 E: 31 F: 26	D: 16 E: 0 F: 0	N/A

5.2.7 M009 (winter day, temperate)

The estimator (Table 24) accurately predicted the most likely condition in 14 of the 19 conditions measured (Table 25). Note that not all conditions occurred during the measurement period (Table 26).

Table 24. Estimator for winter day – temperate.

	Wind Speed (kn)				
Cloud Amount	0	1–5	6–10	11–15	>=16
Clear	C	D	D	D	D
Partly Cloudy	D	C	D	D	D
Mostly Cloudy	D	D	D	D	D
Overcast	D	D	D	D	D

Table 25. Percentage occurrence of Pasquill stability classes from measurements, winter day – temperate.

	Wind Speed (kn)				
Cloud Amount	0	1–5	6–10	11–15	>=16
Clear	A: 0% B: 18% C: 5.2% D: 76.8%	A: 3.4% B: 21.3% C: 38.7% D: 36.6%	A: 0.3% B: 17.6% C: 50% D: 32%	A: 0% B: 6% C: 19 % D: 75.1%	A: 0% B: 1.5% C: 10.2% D: 88.3%
Partly Cloudy	A: 0% B: 0% C: 0% D: 100%	A: 4.2% B: 12.6% C: 34.9% D: 48.4%	A: 0.1% B: 5.3% C: 37.1% D: 57.5%	A: 0% B: 0.5% C: 5.2% D: 94.2%	A: 0% B: 1.5% C: 9.2% D: 89.3%
Mostly Cloudy	A: 0% B: 0% C: 0% D: 100%	A: 0.4% B: 19.6% C: 37% D: 43.1%	A: 0.4% B: 12.7% C: 57% D: 29.9%	A: 0% B: 1% C: 5% D: 94%	A: 0% B: 0% C: 0% D: 100%
Overcast	A: 0% B: 0% C: 0% D: 100%	A: 0% B: 14.4% C: 14.9% D: 70.7%	A: 0% B: 2.9% C: 18.3% D: 78.8%	A: 0% B: 0% C: 18.1% D: 81.9%	N/A

Table 26. Frequency of occurrence of Pasquill stability classes from measurements, winter day – temperate.

	Wind Speed (kn)				
Cloud Amount	0	1–5	6–10	11–15	>=16
Clear	A: 0 B: 69 C: 20 D: 295	A: 87 B: 538 C: 980 D: 926	A: 13 B: 661 C: 1876 D: 1201	A: 0 B: 56 C: 178 D: 705	A: 0 B: 2 C: 14 D: 121
Partly Cloudy	A: 0 B: 0 C: 0 D: 8	A: 33 B: 99 C: 275 D: 381	A: 1 B: 42 C: 294 D: 456	A: 0 B: 2 C: 20 D: 360	A: 0 B: 3 C: 19 D: 184

Cloud Amount	Wind Speed (kn)				
	0	1–5	6–10	11–15	>=16
Mostly Cloudy	A: 0 B: 0 C: 0 D: 52	A: 3 B: 158 C: 298 D: 347	A: 3 B: 86 C: 387 D: 203	A: 0 B: 1 C: 5 D: 94	A: 0 B: 0 C: 0 D: 48
Overcast	A: 0 B: 0 C: 0 D:76	A: 0 B: 194 C: 201 D: 953	A: 0 B: 14 C: 88 D: 378	A: 0 B: 0 C: 21 D: 95	N/A

5.2.8 M009 (winter night, temperate)

The estimator (Table 27) accurately predicted the most likely condition in 10 of the 18 conditions measured (Table 28). Note that not all conditions occurred during the measurement period (Table 29).

Table 27. Estimator for winter night – temperate.

Cloud Amount	Wind Speed (kn)				
	0	1–5	6–10	11–15	>=16
Clear	F	D	D	D	D
Partly Cloudy	F	D	D	D	D
Mostly Cloudy	D	D	D	D	D
Overcast	D	D	D	D	D

Table 28. Percentage occurrence of Pasquill stability classes from measurements, winter night – temperate.

Cloud Amount	Wind Speed (kn)				
	0	1–5	6–10	11–15	>=16
Clear	D: 16.8% E: 82.7% F: 0.5%	D: 36.4% E: 57% F: 6.5%	D: 72.4% E: 25.1% F: 2.5%	D: 100% E: 0% F: 0%	N/A
Partly Cloudy	D: 100% E: 0% F: 0%	D: 41.8% E: 48.9% F: 9.3%	D: 84.5% E: 13.1% F: 2.4%	D: 96.6% E: 2% F: 1.4%	D: 100% E: 0% F: 0%
Mostly Cloudy	D: 21.2% E: 43.3% F: 35.6%	D: 41.8% E: 45% F: 17.8%	D: 68.9% E: 14.8% F: 16.3%	D: 100% E: 0% F: 0%	D: 100% E: 0% F: 0%
Overcast	D: 10.1% E: 81.3% F: 8.6%	D: 28.8% E: 57.4% F: 13.7%	D: 67.1% E: 18.5% F: 14.4%	D: 100% E: 0% F: 0%	N/A

Table 29. Frequency of occurrence of Pasquill stability classes from measurements, winter night – temperate.

Cloud Amount	Wind Speed (kn)				
	0	1–5	6–10	11–15	>=16
Clear	D: 189 E: 933 F: 6	D: 1377 E: 2,155 F: 246	D: 1,680 E: 583 F: 58	D: 40 E: 0 F: 0	N/A
Partly Cloudy	D: 0 E: 176 F: 0	D: 508 E: 595 F: 113	D: 990 E: 153 F: 28	D: 143 E: 3 F: 2	D: 32 E: 0 F: 0
Mostly Cloudy	D: 22 E: 45 F: 37	D: 259 E: 313 F: 124	D: 237 E: 51 F: 56	D: 44 E: 0 F: 0	D: 28 E: 0 F: 0
Overcast	D: 53 E: 426 F: 45	D: 489 E: 974 F: 233	D: 359 E: 99 F: 77	D: 8 E: 0 F: 0	N/A

6 Updates to Noise Assessment Models

6.1 Need for updates

The various noise models (BNoise2, SARNAM, RMTK Noise Tool) have not been substantially updated during the past 10 (or more) years. Due to the archaic and complex form of the interfaces and databases, it is impossible to substantially update the software without performing a major rewrite. Since bug fixes and upgraded capabilities were required, a decision was made to substantially update the models. The update process will not change the underlying science used in the models and where the output of the current models is validated; the updated version will exactly match the output of the previous version.

Updates to the models are being performed to:

- unify the code base across the models;
- ensure that all models have access to the same set of propagation tables;
- update the interface to improve usability to include help tips, to minimize user errors, and to add requested features;
- update the weapon source databases so that all models use the same source data where applicable and to enable corrections and additions to the database; and
- provide full documentation for the users and the developers.

6.2 Justifications for updates

6.2.1 Unify code base

Unifying the code base across the models will enable much more controlled updates and bug fixes. The current models perform largely the same tasks; each has its own base algorithms, but the goals and data differ. While these algorithms are all derived from the same physical principles and behave in similar ways, because they are not fully synchronized, errors in one that may be in others are not always corrected in an efficient manner. This inefficiency is in part due to the current complete separation of the models. Unifying the code base and sharing key portions of the calculation algorithms will enable simpler and more consistent updates across the models. In the process of updating the code, every effort will be taken to streamline, simplify, and modularize the code base.

6.2.2 Add common access to propagation tables

Currently, each of the three models uses a different suite of propagation tables. This has created confusion and occasionally conflicting information for installations and must be corrected. Adding the ability to access all of the propagation tables across the models requires updates to the user interfaces.

6.2.3 Update graphical user interfaces

The graphical user interfaces for BNoise2 and SARNAM have not been updated since the late 1990s to the early 2000s. They currently do not have helpful tips embedded, and the workflow is confusing and not well-documented. As technology has advanced, options for streamlining data input have become available, such as exporting geographical information from an ArcGIS map or exporting RFMSS data into a usable format. The interfaces will be updated to include these options, which will both simplify data entry and minimize user input errors. The workflow of the models is being redesigned to minimize errors, allow easy updating, and reduce data entry time. Without updates to the interfaces, the inclusion of single event propagation tables, which require a "choosing" algorithm, is not possible. Designation of points of interest is a feature that has been manually added to post-process noise contours in the past. Features will be added that allow designation of such points of interest and that will automatically produce a table of resulting noise exposure levels at those points, rather than requiring the user to manually extract that information.

6.2.4 Update weapon source databases

The weapon source databases for BNoise2 and SARNAM must be updated as they currently are locked in the early 2000s state, and new weapons systems cannot be added reliably. The databases are currently open to users, inviting the possibility of incorrect output due to well-meaning but potentially inaccurate user edits. The new versions of the weapon source databases will be locked from editing, other than the additions of custom user input that is occasionally required for experimental weapons system evaluations. The new databases will only be editable by super users or developers, ensuring more reliable data quality. Methods for adding new systems and data will be fully documented.

6.2.5 Improve documentation

The current state of documentation on BNoise2 and SARNAM is severely lacking. SARNAM has a quick-start guide, but no detailed user manual or developer's manual. BNoise2 has no official manual associated with it. The RMTK Noise Tool is well-documented for the user interface, but there is no developer's manual. During the update and unification process, a developer's manual for the unified code base and user manuals—both detailed and quick-guide styles—for each of the models will be fully developed. Helpful tips will be integrated into the updated interfaces.

7 Community Noise Training

The opportunity arose to collaborate with the Navy Facilities Engineering Command (NAVFAC), Atlantic Mission Office on a series of training webinars for community noise. NAVFAC is producing a series of webinars on military noise, and they invited Army elements (U.S. Army Public Health Center Environmental Noise Program and ERDC) to collaboratively develop and deliver material. This collaboration provided a unique opportunity to begin work on the training modules, originally designed for completion in FY19. While this initial work does not fully complete this project's training requirement, it provided an opportunity to begin disseminating basic information on noise to community planners, installation noise points of contact (POCs), and others across the Department of Defense (DoD).

The series of eight webinars was sponsored by NAVFAC and was designed to educate the military installation community on the basics of the impacts of military noise on both installations and the surrounding communities. Participants are encouraged to attend all webinars, as the content progressively builds knowledge. However, attendance at all webinars is not required. A description of the educational goals for each webinar are in Section 7.1–7.8.

7.1 Webinar #1: Introduction to Military Noise (April 13, 2016)

At the end of this lesson, participants should know the following:

- Be familiar with topics and schedule for this noise series.
- Appreciate why noise is an important issue for community plans and liaison officers (CPLOs) and planners to understand.
- Have knowledge of current DoD/Department of Navy (DON) policies and guidance related to noise.
- Have a basic understanding of types of military noise, noise effects, noise science, metrics, and models.
- Be aware of types of noise mitigation options.

7.2 Webinar #2: Noise Metrics and Models (June 16, 2016)

At the end of this lesson, participants should have received the following:

- Have gained a basic understanding of primary and supplemental noise metrics and when each type of metric should be used.

- Be aware of various presentation options for metrics.
- Be familiar with types and purposes for environmental noise models.
- Understand federal guidance and policies related to noise models and metrics.
- Have talking points for communication of noise metrics and models to the public.

7.3 Webinar #3: Noise Studies (August 16, 2016)

At the end of this lesson, participants should have learned the following:
- Recognize when and why noise studies are completed.
- Understand what noise study guidance and resources are available.
- Become acquainted with noise modeling vs. monitoring, and when to use each.
- Become familiar with the noise study process, including data needs, data collection procedures, validation, and review.

7.4 Webinar #4: Range Noise (October 12, 2016)

At the end of this lesson, participants should have the following knowledge:
- Become familiar with the various sources of range noise.
- Understand how range noise sources are different from other types of sources.
- Recognize the unique characteristics of range noise.
- Know current policies and guidance related to range noise.
- Understand the process for assessing range noise.

7.5 Webinar #5: Reducing Noise Conflict (December 8, 2016)

At the end of this lesson, participants should have learned the following:
- Become aware of the various types of techniques to reduce and/or mitigate noise exposure.
- Understand how changes at the source, path, and receiver can affect noise levels and community exposure.

7.6 Webinar #6: Response to Noise Inquiries and Noise Complaint Management (February 14, 2017)

At the end of this lesson, participants should know the following:
- Understand public response to noise and why noise inquiries and complaints occur.

- Appreciate reasons to respond to noise inquiries and manage complaints.
- Be aware of tools and methods for noise response.
- Understand lessons learned in noise response and communication.

7.7 Webinar #7: Introduction to Underwater Acoustics (March 2, 2017)

At the end of this lesson, participants should have learned the following:

- Become familiar with the various types and sources of underwater sounds.
- Have a basic understanding of the metrics and models used to describe underwater sound.
- Understand current DoD/DON policies related to underwater sound;
- Have a basic understanding of the impacts of underwater sound on the National Environmental Policy Act (NEPA) and Endangered Species Act (ESA)/Marine Mammal Protection Act (MMPA) consultation processes.

7.8 Webinar #8: Implementation of Noise Compatibility Tools & Guidelines (April 12, 2017)

At the end of this lesson, participants should have learned the following:

- Become familiar with federal land use compatibility guidelines related to noise.
- Have a basic understanding of tools for implementing land use guidelines.
- Understand how federal guidelines are implemented within DoD's compatible use programs and NEPA.

8 Summary

To date, the ESOH Short-Term Noise Assessment Demonstration/Validation project has made excellent progress toward validating and improving the noise assessment tools available for range noise in the DoD. In FY16, several avenues and tasks were completed or commenced, as listed below.

- An automated methodology was developed and implemented for generating the noise assessment tool outputs that are required for comparison to experimental data. This methodology will be further expanded to accommodate real training range noise in FY17.
- Statistical analysis was completed of a comparison between the benchmark dataset (ERDC Long-Range Sound Propagation Dataset) and the model outputs for corresponding meteorological conditions. This analysis found that the models are consistently underpredicting the received levels (~62% of the time), based on the benchmark dataset. Investigations into possible errors in the noise model codes and a determination of the optimal set of propagation classes to use is ongoing in FY17.
- The peak-level calculation algorithm and comparison of results to other methodologies were completed. This study found that the peak-level method currently in use may be improved by using alternative methods.
- An analysis was completed of the meteorological conditions and their mapping to selected propagation conditions within the noise models. This study found that there is potentially significant variability in propagation conditions across a given landscape. It also found that the "quick" method for choosing which propagation condition to use for general weather conditions is only correct about 50% of the time. These two results indicate that other avenues should be explored for classifying the propagation conditions, and an alternative method should be developed for determining which propagation condition to use for a single event noise assessment. Both of these tasks are ongoing in FY17.
- Progress toward updating the noise assessment models is proceeding. An updated interface design that will enable all models to access the same set of propagation tables is nearing finalization. Opportunities for unifying the underlying calculation engine code are under investigation, and the existing code is being fully analyzed for accuracy. The updates and bug fixes are expected to be completed by Q3FY18.

- The Army is participating in Navy-sponsored webinar training on community noise assessment, policy, and mitigation. This activity provided an excellent baseline for ERDC's planned FY19 training specifically on short-term noise assessment.

Abbreviations

Term	Meaning
ASA (IE&E)	Assistant Secretary of the Army for Installations, Energy and Environment
ASOS	Automated Surface Observing Stations
BNoise 2	Blast Noise Version 2
CONUS	continental United States
CPLO	community plans and liaison officers
CSEL	C-weighted sound exposure level
dB	decibel
DoD	Department of Defense
DON	Department of Navy
ERDC	Engineer Research and Development Center
ERDC-CERL	Engineer Research and Development Center–Construction Engineering Research Laboratory
ESA	Endangered Species Act
ESOH	Environment, Safety and Occupational Health
FY	fiscal year
L_{pk}	Peak Level (dB)
MMPA	Marine Mammal Protection Act
NAVFAC	Navy Facilities
NEPA	National Environmental Protection Act
P-G	Pasquill-Gifford
PK15	Peak Level exceeded 15% based on meteorological variability
POC	point of contact
RMTK	Range Managers Toolkit
SARNAM	Small Arms Range Noise Assessment Model
SRD-T	Solar Radiation Delta-T
SEL	sound exposure level

References

Army Regulation 200-1. December 2007. Environmental Protection and Enhancement, Chapter 14, "Operational Noise," 44–45. Washington, DC: Department of the Army.

Coulter, C.T. 1993. *An Evaluation of a Solar Radiation/Delta-T Method for Estimating Pasquill-Gifford (P-G) Stability Categories*. EPA report 454/R-93-055. Research Triangle Park, NC: U.S. EPA, Office of Air Quality Planning and Standards.

Lewin-Koh, Nicholas. 2011. "Hexagon Binning: An Overview." https://cran.r-project.org/web/packages/hexbin/vignettes/hexagon_binning.pdf

Pasquill, Frank. 1974. *Atmospheric Diffusion,* 2nd ed. New York, NY: Halsted Press.

Pater, Larry, Jeffery Mifflin, Kristy A. Broska, and William A. Russell. 2007. *SARNAM™ Noise Impact Software*. Final Report for ESTCP Project SI-0006: "Assessing and Controlling Blast Noise Emission." Alexandria, VA: Environmental Security Technology Certification Program.

Pater, Larry, Michael J. White, Donald G. Albert, Michelle E. Swearingen, D. Keith Wilson, Edward T. Nykaza, Bruce MacAllister, Jeff Mifflin, Bonnie Jones, Dan Valente, and Sarah Nemeth. March 2017. *High Energy Large Scale Blast Sound Propagation Experiments*. ERDC/CERL TR-17-8. Champaign, IL: Engineer Research and Development Center, Construction Engineering Research Laboratory (ERDC-CERL).

Razali, N.M. and Y.B. Wah. 2011. "Power Comparisons of Shapiro-Wilk, Kolmogorov-Smirnov, Lilliefors, and Anderson-Darling Tests." *Journal of Statistical Modeling and Analytics* 2(1): 21–33.

Rodgers, Joe L., and W. Alan Nicewander. 1988. "Thirteen Ways to Look at the Correlation Coefficient." *The American Statistician* 42(1): 59–66.

Swearingen, Michelle E. 2006. *The Range Managers Toolkit (RMTK) Noise Tool*. ERDC/CERL TR-06-15. Vicksburg, MS: Engineer Research and Development Center.

Swearingen, Michelle E. Accessed 2017. "Blast Noise Impact Assessment (BNOISE2)." In the "Noise Impact Model factsheet." Vicksburg, MS: Engineer Research and Development Center. http://www.erdc.usace.army.mil/Media/Fact-Sheets/Fact-Sheet-Article-View/Article/476733/noise-impact-model/.

Valente, Daniel P., Lauren M. Ronsse, Larry Pater, Michael J. White, Roger Serwy, Edward T. Nykaza, and Michelle E. Swearingen. 2012a. "Blast Noise Characteristics as a Function of Distance for Temperate and Desert Climates." *Journal of the Acoustical Society of America* 132(1): 216–227.

Valente, Daniel P., Lauren Ronsse, Roger D. Serwy, Jesse Barr, Keran Claffey, Michael J. White, and Michelle E. Swearingen. 2012b. *Data Preparation Procedures for the ERDC High-Energy Large-Scale Blast Sound Propagation Experiment*. ERDC TR-12-12. Vicksburg, MS: Engineer Research and Development Center.

White, Michael J. January 2002. “Peak Level Algorithm.” ARA Project 0925. Littleton, CO: Applied Research Associates, Inc.

REPORT DOCUMENTATION PAGE

Form Approved
OMB No. 0704-0188

1. REPORT DATE (DD-MM-YYYY)	2. REPORT TYPE	3. DATES COVERED (From - To)
June 2017	Final Technical Report	

4. TITLE AND SUBTITLE

Validation of Short-Term Noise Assessment Procedures: FY16 Summary of Procedures, Progress, and Preliminary Results

5a. CONTRACT NUMBER

5b. GRANT NUMBER

5c. PROGRAM ELEMENT NUMBER

E21

6. AUTHOR(S)

Michelle E. Swearingen, Gregory W. Lyons, Kate A. Morozova, Andrew R. Lammers, Brian R. Greene, Michael J. White, Lacey S. Duckworth, and Jesse M. Barr

5d. PROJECT NUMBER

5e. TASK NUMBER

5f. WORK UNIT NUMBER

Work Unit 2JF1C8

7. PERFORMING ORGANIZATION NAME(S) AND ADDRESS(ES)

U.S. Army Engineer Research and Development Center (ERDC)
Construction Engineering Research Laboratory (CERL)
PO Box 9005
Champaign, IL 61826-9005

8. PERFORMING ORGANIZATION REPORT NUMBER

ERDC TR-17-6

9. SPONSORING / MONITORING AGENCY NAME(S) AND ADDRESS(ES)

Assistant Secretary of the Army
for Installations, Energy and Environment
110 Army Pentagon, Room 3E464
Washington, DC 20310-0110

10. SPONSOR/MONITOR'S ACRONYM(S)

ASA(IE&E)

11. SPONSOR/MONITOR'S REPORT NUMBER(S)

12. DISTRIBUTION / AVAILABILITY STATEMENT

Approved for public release. Distribution is unlimited.

13. SUPPLEMENTARY NOTES

14. ABSTRACT

Army regulations require that installations assess the impacts of training range noise on wildlife and the human community. This work pro-vides a summary of the work performed in fiscal year 2016 for the Environment, Safety and Occupational Health Short-Term Noise Assessment Procedure Demonstration/Validation project. This report describes the procedure used to generate the noise models' output dataset, and then it compares that dataset to the benchmark, the Engineer Research and Development Center's Long-Range Sound Propagation dataset. It was found that the models consistently underpredict the measured values. Multiple topics were explored towards identifying possible sources of error. The peak-level calculation algorithm is found to perform adequately, but an alternative method is recommended for future use. Significant meteorological variability is found across the landscape, leading to challenges in estimating the correct propagation class for a particular scenario. A deeper investigation of the propagation class selection algorithm is continuing in FY17. Updates to the noise assessment tools are identified. Throughout this document, procedures used for calculations and analysis are included.

15. SUBJECT TERMS

Military Bases–Noise–Computer simulation, Noise control, Forensic accoustics, Computer programs–Verification

16. SECURITY CLASSIFICATION OF:			17. LIMITATION OF ABSTRACT	18. NUMBER OF PAGES	19a. NAME OF RESPONSIBLE PERSON
a. REPORT	b. ABSTRACT	c. THIS PAGE			19b. TELEPHONE NUMBER (include area code)
Unclassified	Unclassified	Unclassified	UU	66	